Prefrontal layer V pyramidal neurons comprise multiple subtypes with distinct nicotinic responses and projection targets

Ashutosh V. Patel[1], Anthony Nguyen[1], Pietro Paletta[2], Elena Choleris[2] and Craig D.C. Bailey[1]*

[1]Department of Biomedical Sciences, University of Guelph, Guelph, ON, Canada, [2]Department of Psychology, University of Guelph, Guelph, ON, Canada

*email: baileyc@uoguelph.ca

Abstract

Pyramidal neurons located within layer V of the medial prefrontal cortex drive cognitive circuits by integrating afferent signals and sending efferent projections to cortical and subcortical targets. This role is supported by cholinergic neurotransmission, which modulates pyramidal neuron excitability via postsynaptic nicotinic receptors. We employed whole-cell electrophysiology with neuron reconstruction in brain slices from mice of both sexes to demonstrate that medial prefrontal layer V pyramidal neurons comprise three subtypes that have distinct electrophysiological properties, receptor isoform-specific nicotinic responses, and projection targets. Burst-firing neurons may be sub-divided into subtypes having (i) α7 isoform nicotinic responses and projections to the contralateral cortex, or (ii) α7 and β2 isoform nicotinic responses and projections to the nucleus accumbens. Regular-firing neurons have β2 isoform nicotinic responses and projections to the ventromedial thalamus. These findings provide new insight into an isoform-specific mechanism by which cholinergic neurotransmission modulates distinct efferent projections from this cognitive brain region.

Introduction

The modulatory neurotransmitter acetylcholine (ACh) acts within the rodent medial prefrontal cortex (mPFC) to support goal-directed cognitive functions such as working memory and attention[1-5]. The manner by which ACh fulfills this role is sophisticated and likely multimodal[6,7], as evidence exists for both a sustained tonic increase in extracellular ACh content[8-10] and a transient phasic increase in synaptic ACh content[2,3] for animals performing visual attention tasks. It is known that ACh activation of its nicotinic class of receptor (nAChR) plays an important role in this process because the pharmacological or genetic disruption of nAChR function impairs performance on mPFC-dependent cognitive tasks[4,5,11,12]. The nAChR comprises a group of pentameric ligand-gated ion channels that are permeable to monovalent and divalent cations. The two predominant nAChR isoforms within the mPFC are homomeric α7 nAChRs (composed of five α7 subunits) and heteromeric β2 nAChRs (composed of α4 and β2 subunits with the potential addition of one α5 subunit). These isoforms possess distinct functional properties and are differentially expressed within cellular layers and neuron types of the mPFC[4,13-15]. Within layer V of the mPFC, it has been established that pyramidal neurons express α7 nAChRs, fast spiking interneurons express α7 nAChRs, and non-fast spiking interneurons express β2 nAChRs[15]. However, evidence suggests that layer V pyramidal neurons within other cortical regions express both α7 and β2 nAChRs[16]. It is important to determine whether layer V pyramidal neurons within the mPFC also express both receptor isoforms because this will further our understanding of the sophisticated manner by which cholinergic neurotransmission supports mPFC cognitive circuits.

Layer V pyramidal neurons integrate inputs from cortical and subcortical sources, placing them in an important position to drive cognitive signaling. Although these neurons show physiological and morphological heterogeneity, multiple schemata have been designed which categorize neurons into subtypes based on electrophysiological and/or morphological

properties. The two broad electrophysiological subtypes comprise intrinsically burst firing (BF) neurons, which show bursts with a short interspike interval (ISI) at the beginning of a train of action potentials, and regular firing (RF) neurons, which show a relatively consistent and longer ISI throughout a train of action potentials[17-23]. Depending on the cortical region, intrinsic electrophysiological properties have been demonstrated to differ between BF and RF neurons[17,20,24]. Also depending on the cortical region, the morphology of the apical dendrite tuft also differs between BF and RF neurons. Within primary sensory cortices, it has been shown most often that BF neurons have a broader apical tuft with more dendrite matter[20,21]. Within the mPFC, the opposite has been found such that BF neurons have a thinner tuft and less dendrite matter[17]. The determination of neuron projections from primary sensory cortices shows a dissociation between neuron subtypes such that that BF neurons project to the cerebral cortex and striatum whereas RF neurons project to the cerebral cortex and thalamus[25,26]. The projection targets of layer V pyramidal neuron subtypes within the mPFC are not known.

This present study identifies and characterizes three pyramidal neuron subtypes within layer V of the juvenile mouse mPFC that have distinct electrophysiological, morphological, and projection properties. BF neurons projecting to the contralateral mPFC show α7 nAChR responses; BF neurons projecting to the ipsilateral striatum show a combination of α7 and β2 nAChR responses; and RF neurons projecting to the ipsilateral thalamus show β2 nAChR responses. To our knowledge, these findings are the first to demonstrate that distinct pyramidal neuron subtypes within layer V of the mPFC project to unique cortical and subcortical targets. Moreover, these findings provide new insight into an nAChR isoform-specific mechanism by which cholinergic neurotransmission modulates distinct efferent projections from this cognitive brain region.

Results

Layer V pyramidal neuron subtypes have distinct nicotinic responses. Pyramidal neurons within layer V of the prelimbic cortex may first be categorized into two broad subtypes based on their pattern of action potential firing in response to 200 pA of depolarizing current for 500 ms (Fig. 1). Like pyramidal neurons in other layers and regions[19,27], we identified a subtype of BF neurons based on a short initial ISI between the first two action potentials of <10 ms and a subtype of RF neurons based on a relatively longer ISI between the first two action potentials of >10 ms. The BF subtype may be further divided based on the nicotinic responses that were observed. Pressure application of 1 mM ACh for 100 ms approximately 50 μm lateral to the soma elicited two distinct types of responses in BF neurons having either a fast rise and fast decay (Fig. $1a_2$) or a fast rise and two-phase fast and slow decay (Fig. $1b_2$). Responses with a fast rise and fast decay were not affected by the β2 nAChR antagonist dihydro-β-erythroidine (DHβE) but were blocked completely by the α7 nAChR antagonist methyllycaconitine (MLA) (Fig. 1a), which is consistent with previous reports that α7 nAChRs are present on cortical layer V pyramidal neurons[16]. Responses with a fast rise and two-phase decay had fast components blocked by MLA and the remaining slow components blocked by DHβE (Fig. 1b), suggesting the presence of both α7 and β2 nAChRs, and possibly also the presence of α7β2 heteromer nAChRs[28] (referred to herein as α7/β2 responses). This same ACh application to RF neurons consistently elicited responses with a slow rise and slow decay that were characteristic of β2 nAChRs[5,29]. This was confirmed pharmacologically, as these responses were unaffected by MLA but were blocked completely by DHβE (Fig. 1c). Contingency analysis revealed that approximately half of prelimbic layer V neurons are BF and modulated by α7 responses only (Male: 29/57; Female: 35/63), approximately one-quarter of neurons are BF and modulated by α7/β2 responses (Male: 13/57; Female: 15/63), and approximately one-quarter of neurons are RF and modulated by β2 responses only (Male: 15/57; Female: 13/63) (Fig. 1d). These

distributions did not differ between sexes (Chi-square test, $p = 0.76$).

Previous studies have characterized the kinetics of nicotinic responses mediated by α7, α7β2 and β2 nAChRs[30,31]. We measured the kinetics of the three nAChR response types in the three pyramidal neuron subtypes by fitting current responses to an eight-term Fourier series equation (Fig. 2). Current amplitude (Fig. 2a) differed amongst response types (two-way ANOVA, $F(2,112) = 16.29$, $p < 0.0001$) with α7 responses having a greater amplitude than α7/β2 and β2 responses in males and β2 responses in females (Bonferroni *post hoc* correction, each $p < 0.01$). The net charge (Fig. 2b) differed amongst response types ($F(2,114) = 64.61$, $p < 0.0001$ with the β2 response having greater net charge than α7 and α7/β2 responses in both sexes (each $p < 0.01$). The time to the peak response (Fig. 2c) differed amongst response types ($F(2,114) = 196.10$, $p < 0.0001$ with the β2 response having a greater time to peak than α7 and α7/β2 responses in both sexes (each $p < 0.0001$). Similarly, rise tau (Fig. 2d) differed amongst response types ($F(2,114) = 84.42$, $p < 0.0001$ with the β2 response having a greater rise tau than α7 and α7/β2 responses in both sexes (each $p < 0.0001$). The first decay tau (Fig. 2e) differed amongst response types ($F(2,114) = 418.80$, $p < 0.0001$ with the β2 response having a greater first decay tau than α7 and α7/β2 responses in both sexes (each $p < 0.0001$). This measure also differed between α7 and α7/β2 responses in females only ($p < 0.01$). The second decay tau (Fig. 2f) differed amongst response types ($F(2,114) = 361.60$, $p < 0.0001$ and reliably differentiated the three response types, as each was different than the other in both sexes (each $p < 0.0001$). This measure is particularly sensitive to differentiating α7 and α7/β2 responses, as the second decay tau was less than 1000 ms for α7 responses and greater than 1000 ms for α7/β2 responses. These analyses demonstrate that nicotinic responses mediated by α7, α7/β2, and β2 nAChRs have distinct activation and desensitization kinetics within the three pyramidal neuron subtypes.

Intrinsic electrophysiological properties of layer V pyramidal neuron subtypes. The distinct electrophysiological properties of BF and RF pyramidal neurons have been characterized in hippocampal and cortical sub-regions[17,27,32,33]. We analyzed the intrinsic electrophysiological properties of the layer V pyramidal neurons of this study in relation with their α7, α7/β2, and β2 nicotinic responses (Fig. 3). Two-way ANOVA demonstrated that resting membrane potential does not differ between neuron subtypes ($F(2,114) = 2.33$, $p = 0.1$) or sexes ($F(1,114) = 0.25$, $p = 0.6$). Membrane resistance (Fig. 3a) was affected by neuron subtype ($F(2,114) = 29.26$, $p < 0.0001$) with resistance being greater in RF (β2) neurons than in each of the BF subtypes (Bonferroni *post hoc* correction, each $p < 0.001$). As expected, ISI ratio (Fig. 3b) was affected by neuron subtype ($F(2,113) = 46.71$, $p < 0.0001$) with the ISI ratio being greater in RF (β2) neurons than in each of the BF subtypes (each $p < 0.001$). Rheobase (Fig 3c) showed an effect of neuron subtype ($F(2,113) = 5.10$), $p = 0.008$) although sag ratio (Fig 3d) did not $F(2,114) = 2.67$, $p = 0.07$). Additional analyses revealed differences in active electrophysiological properties between neuron subtypes. For example, within input/output experiments RF (β2) neurons exhibited greater excitability and a noticeable depolarization block in both sexes (Fig. 3e-f). The magnitude of the post-firing afterhyperpolarization (AHP), which influences excitability, also differed between neuron subtypes. In both sexes, there was a significant interaction between the number of action potentials and AHP magnitude (Fig. 3g-h). Overall, these analyses demonstrate that the passive and active intrinsic electrophysiological properties differ between layer V pyramidal neuron subtypes, with the two BF subtypes being similar to each other but different from the RF (β2) subtype.

Excitatory presynaptic input to layer V pyramidal neuron subtypes. A major source of glutamatergic input to layer V of the mPFC originates from the thalamic nuclei[34]. We measured the properties of spontaneous excitatory postsynaptic currents (EPSCs) received by neurons

within the three pyramidal neuron subtypes. EPSC frequency (Fig. 4a) was affected by neuron subtype (two-way ANOVA, $F(2,113) = 13.41$, $p < 0.0001$), with frequency in both sexes being lower in RF (β2) neurons than BF (α7) neurons (Bonferroni post hoc correction, $p < 0.01$). Similarly, both EPSC amplitude (Fig. 4b, $F(2,112) = 10.31$, $p < 0.0001$) and net charge (Fig. 4c, $F(2,113) = 17.26$, $p < 0.0001$) were affected by neuron subtype with values in both sexes being lower in RF (β2) neurons than in BF (α7) neurons (all $p < 0.01$). There was no sex difference for EPSC frequency ($F(1,113) = 0.35$, $p = 0.6$) but there were sex differences for both EPSC amplitude ($F(1,112) = 20.34$, $p < 0.0001$) and net charge $F(1,113) = 19.91$, $p < 0.0001$) in that values were greater in males than females. These results suggest that glutamatergic signaling received within layer V of the mPFC differs depending on pyramidal neuron subtype.

Correlation between electrophysiological properties and nicotinic responses. Correlation analyses were performed for all neurons within each sex, to assess relationships between eight intrinsic electrophysiological properties, four measures of nicotinic currents, and three measures of EPSCs. Fig. 5a. shows the resulting correlation matrix for each sex, with positive correlations marked green and negative correlations marked red. Multiple positive correlations were identified that could be expected based on group differences between pyramidal neuron subtypes. For example, membrane resistance (which was greatest in RF (β2) neurons) correlated positively with interspike interval adaptation ratio and input/output excitability (which were both greatest in RF (β2) neurons). Membrane resistance also correlated positively with measures of nicotinic response kinetics, which were all slower in RF (β2) neurons. Correlations were identified between measures of nicotinic responses and EPSCs that were not expected. For example, measures of nicotinic response kinetics correlated negatively with EPSC frequency but correlated positively with EPSC amplitude and EPSC net charge.

We next measured potential clustering of recorded neurons using a principal

component analysis, for which each of the 17 electrophysiological properties, nicotinic response, and EPSC properties from the correlation analyses were treated as principal components (PCs). Neurons from male mice had four PCs and neurons from female mice had six PCs with eigenvalues greater than 1, which accounted for 74.2% and 83.2% of the total variance, respectively. A screeplot was used to confirm that a plateau was reached with these PCs and that the remaining PCs did not significantly contribute to group variance. The three PCs with the greatest contribution toward group variance accounted for 37.0%, 15.9%, and 13.1% of total variance in males and 33.4%, 15.1%, and 11.5% of the total variance in females. In both the sexes, the measures that largely contributed to the first PC are nicotinic peak response amplitude (Male: 0.13; Female: 0.14), rise tau (Male: 0.10; Female: 0.12), 1st decay tau (Male: 0.13; Female: 0.14) and 2nd decay tau (Male:0.12; Female: 0.10). Fig. 5b shows three-dimension plots of neurons positioned according to the three largest PCs. Here, neurons separated into two distinct clusters comprising the BF (α7 and α7/β2) neurons or RF (β2) neurons. For the BF neuron subtypes, BF (α7) neuron positions were more elongated along the PC2 and PC3 axes, whereas the BF (α7/β2) neurons formed a tighter cluster within all three axes.

Distinct morphologies of layer V pyramidal neuron subtypes. The morphology of layer V pyramidal neurons is highly heterogenous[17] and developmentally regulated[35]. The morphology of neighbouring mPFC layer VI neurons has been related previously with muscarinic[13] and nicotinic[36] responses, so we next sought to measure the morphology of the three layer V pyramidal neuron subtypes in this current study. Sholl type plots were prepared for a random subset of neurons within each sex that were labelled and analysed based on dendrite length (Fig. 6a,b), diameter (Fig. 6c,d), and volume (Fig 6e,f).

Apical dendrite length showed opposite effects of neuron subtype in each sex. In males,

there was a significant effect of neuron type (two-way ANOVA, $F(2,520) = 11.99$, $p < 0.0001$) with BF ($\alpha7$) neurons having a smaller length than the other two neuron types (Bonferroni post hoc correction, each $p < 0.01$). In females, there was a significant effect of neuron type ($F(2,506) = 16.52$, $p < 0.0001$) with BF ($\alpha7$) neurons having a greater length than the other two neuron types (each $p < 0.0001$). Basal dendrite length showed similar effects of neuron subtype within males ($F(2,380) = 41.55$, $p < 0.0001$) and females ($F(2,414) = 8.82$, $p = 0.0002$). In both sexes, BF ($\alpha7$) neurons had the greatest basal dendrite length and RF ($\beta2$) neurons had the smallest basal dendrite length. All neuron subtypes were different from each other (each $p < 0.05$) except for the two BF subtypes within females.

Apical dendrite diameter showed opposite effects of neuron subtype in each sex. In males, there was a significant effect of neuron type ($F(2,520) = 20.81$, $p < 0.0001$) with BF ($\alpha7$) neurons having a smaller diameter than the other two neuron types (each $p < 0.001$). In females, there was a significant effect of neuron type ($F(2,506) = 53.13$, $p < 0.0001$) with BF ($\alpha7$) neurons having a greater diameter than the other two neuron types (each $p < 0.0001$). Basal dendrite diameter showed an effect of neuron subtype within males ($F(2,380) = 16.65$, $p < 0.0001$) with BF ($\alpha7$) neurons having a greater diameter than the other two neuron subtypes (each $p < 0.05$). Basal dendrite diameter was not affected by neuron subtype in females ($F(2,414) = 1.60$, $p = 0.2$).

Apical dendrite volume showed opposite effects of neuron subtype in each sex. In males, there was a significant effect of neuron type ($F(2,520) = 14.19$, $p < 0.0001$) with BF ($\alpha7$) neurons having a smaller volume than BF ($\alpha7/\beta2$) neurons ($p < 0.0001$). In females, there was a significant effect of neuron type ($F(2,506) = 65.19$, $p < 0.0001$) with BF ($\alpha7$) neurons having a greater volume than the other two neuron types (each $p < 0.0001$). Basal dendrite volume showed similar effects of neuron subtype within males ($F(2,380) = 18.79$, $p < 0.0001$) and females ($F(2,414) = 25.46$, $p < 0.0001$), with RF ($\beta2$) neurons having a smaller basal dendrite

volume than the other two neuron subtypes (each $p < 0.001$).

Sex differences within layer V pyramidal neuron subtypes. Sex differences have been identified for pyramidal neuron morphology within mPFC layer VI[13]. Here, we performed a direct comparison of dendrite volume between male and female pyramidal neurons sampled from each subtype. The most striking sex difference was observed for BF (α7) neurons, where apical (two-way ANOVA, $F(1,468) = 110.20$, $p < 0.0001$) and basal ($F(1,342) = 5.57$, $p = 0.02$) dendrites had a greater volume in females (Fig. 7a). On the contrary, there was no sex difference for BF (α7/β2) neuron apical ($F(1,213) = 3.69$, $p = 0.06$) or basal ($F(1,228) = 0.03$, $p = 0.9$) dendrites (Fig. 7b). There were subtle sex differences in RF (β2) neurons, where apical dendrites had a greater volume in males ($F(1,338) = 4.77$, $p = 0.03$) and basal dendrites had a greater volume in females ($F(1,247) = 11.82$, $p = 0.0007$) (Fig. 7c). These results demonstrate that the morphology of some mPFC layer V pyramidal neuron subtypes is sex specific during the juvenile period, suggesting the potential for distinct developmental trajectories.

Layer V pyramidal neuron subtypes project to unique brain regions. Previous work has shown that neocortical neurons projecting to unique brain regions have distinct electrophysiological properties[25,37]. We next sought to determine whether the mPFC layer V pyramidal neuron subtypes identified in this current study project to unique brain regions using retrograde labeling approach. A retrograde tracer was injected into the contralateral mPFC, ipsilateral nucleus accumbens, or ipsilateral ventromedial thalamus in mice of both sexes at P18 and labeled mPFC layer V pyramidal neurons were recorded for whole cell electrophysiology at P21. Neurons were recorded from 3-4 mice per projection target per sex. The results from this experiment confirm that each neuron subtype projects to a unique target. All recorded corticocortical neurons projecting to the contralateral mPFC had electrophysiological properties

consistent with the BF (α7) subtype (Fig. 8a), as they exhibited a BF response to positive current injection and a nicotinic response with a fast onset and one-component fast decay. These properties were observed in 10/10 neurons from males and 10/10 neurons from females. All recorded corticostriatal neurons projecting to the nucleus accumbens had electrophysiological properties consistent with the BF (α7/β2) subtype (Fig. 8b), as they exhibited a BF response to positive current injection and a nicotinic response with a fast onset and two-component fast + slow decay. These properties were observed in 10/10 neurons from males and 10/10 neurons from females. In a separate set of animals, retrograde labelling showed that neurons projecting to the caudate/putamen, basolateral amygdala, and lateral hypothalamus also all had electrophysiological properties consistent with the BF (α7/β2) subtype (data not shown), suggesting that this neurons from this subtype may project to multiple targets. All recorded corticothalamic neurons projecting to the ipsilateral ventromedial thalamus had electrophysiological properties consistent with the RF (β2) subtype (Fig. 8c), as they exhibited a RF response to positive current injection and a nicotinic response with a slow onset and one-component slow decay. These properties were observed in 12/12 neurons from males and 12/12 neurons from females. To our knowledge, these collective findings demonstrate for the first time that distinct mPFC layer V pyramidal neurons subtypes project to unique cortical and subcortical targets.

Discussion

Layer V pyramidal neurons play a central role within mPFC cognitive circuits. They span the cortical column, integrate afferent signals from cortical and subcortical sources[38], and send efferent signals to cortical and subcortical targets[39]. Their role to support cognitive functions is shaped by cholinergic neurotransmission that involves postsynaptic nicotinic responses[15,16,40]. Determining the precise manner by which nicotinic signalling modulates mPFC layer V neurons is key to understanding the sophisticated role of cholinergic neurotransmission to support mPFC cognitive circuits. In this present study, we report the following for mPFC layer V pyramidal neurons: 1) BF and RF neurons exhibit distinct nicotinic responses mediated by α7 and/or β2 subunit-containing nAChR isoforms; 2) these neuron subtypes, containing distinct nicotinic responses, exhibit distinct intrinsic electrophysiological and morphological properties; 3) these neuron subtypes exhibit distinct levels of spontaneous glutamatergic input; 4) strong correlations exist between certain intrinsic electrophysiological properties and measures of nicotinic responses; and 5) these neuron subtypes project to distinct and mutually exclusive targets within the brain. A graphical summary of these findings is presented in Fig. 9.

The functional presence of nAChR isoforms has been characterized previously for specific neuron types within each layer of the rodent mPFC[15,36,41-44]. That work shows α7 nAChRs to be present on fast spiking and non-fast spiking interneurons within layers I, II/III, and V, and on pyramidal neurons within layer V only[15,42-44]. It also shows β2 nAChRs to be present on thalamocortical glutamatergic terminals within layer V[34], fast spiking interneurons within layer V[41], non-fast spiking interneurons within all layers[15,44], and on pyramidal neurons within layer VI only[4,15,36]. Considering this previous work, we were surprised to observe responses mediated by β2 subunit-containing nAChRs in approximately half of the morphologically confirmed mPFC layer V pyramidal neurons from this current study. Specifically, we observed α7/β2 nicotinic responses in approximately half of BF pyramidal neurons and β2 nicotinic responses in all RF

pyramidal neurons (Fig. 1d). The previous research described above was performed using mice and rats of approximately the same age as those in our study but was performed at a greater recording temperature than our study. Although recording temperature can influence BF and RF patterns for pyramidal neurons[18], we have found that it does not influence apparent nAChR isoform-specific responses within the pyramidal neurons of our study. Another variable that may differ between our study and previous research is the mPFC sub-region from which neurons were sampled (e.g., the prelimbic or infralimbic regions). Neurons in our study were sampled from the prelimbic region only, whereas the sub-regions from which neurons were sampled in previous studies are not commonly reported. Consistent with our findings, β2 nicotinic responses have been observed previously in layer V pyramidal neurons located within the rat somatosensory[16] and mouse auditory[45] cortices.

Pyramidal neurons within layer V of the cerebral cortex exhibit a diverse set of electrophysiological properties[18,21,36,46–48]. Like previous work in the mPFC and other cortical regions, we can first categorize the layer V neurons from this study into BF and RF subtypes. To the best of our knowledge, we now show for the first time that receptor isoform-specific nicotinic responses map onto theses neuron subtypes within layer V of the mPFC. Principal component analysis of the electrophysiology data collected from these neurons (Fig. 5) confirmed the separation of BF (α7 and α7/β2) and RF (β2) subtypes, although the BF subtype could not be further separated based on its α7 versus α7/β2 responses. This neuron subtype-specific expression of nAChR isoforms may be unique to the mPFC, as both α7 and β2 responses have been observed in RF neurons within layer V of the somatosensory cortex[16]. The output from prefrontal BF neurons is thought to synchronize this region during attention tasks[46,47]. Given the likely contribution of both phasic[7] and tonic[6] acetylcholine neurotransmission toward attention, our results suggest that, within layer V of the mPFC, α7 subunit-containing nAChRs on BF

neurons may mediate short term cue detection whereas β2 nAChRs on RF neurons may play a more modulatory role to enhance global attention.

Pyramidal neurons within layer V of the cerebral cortex exhibit a highly heterogeneous morphology that has been related with their electrophysiological properties[17,48-50]. BF and RF neurons are known to have different morphological properties with the general finding that BF neurons have a greater dendrite arborization[21,24,51]. Moreover, the BF pattern originates from dendritic stimulation whereas the RF pattern originates from somatic stimulation[52]. This is consistent with our finding that BF (α7) neurons exhibit a greater EPSC frequency, amplitude, and net charge than RF (β2) neurons in both sexes, suggesting that these pyramidal neuron subtypes are modulated differentially by presynaptic input. Layer V pyramidal neurons have been categorized previously as having either broad tufted, slender tufted, or untufted apical dendrites[17,49]. Like previous reports within layer VI of the mPFC[13,36], we demonstrate that cholinergic responses are related with pyramidal neuron morphology in a sex-dependent manner within layer V of the mPFC during the juvenile period of postnatal development. α7 responses map on to untufted neurons in male mice and broad tufted neurons in female mice, whereas α7/β2 responses map onto broad tufted neurons in male mice and untufted neurons in female mice. β2 responses map onto slender tufted neurons in both sexes. Although cholinergic signalling influences pyramidal neuron morphology within other layers of the mPFC[36,53], it cannot be determined based on our data whether the distinct nAChR isoforms play a role to shape the morphology of the pyramidal neuron subtypes identified within layer V in this study.

The most striking sex difference observed in this study is the greater dendrite length and volume measured in BF (α7) neurons from female mice (Fig. 7a) which, unexpectedly, is not consistent with the greater EPSC amplitude and net charge measured in BF (α7) neurons from male mice. Other measures of intrinsic electrophysiological properties that may reflect neuron size (e.g. membrane resistance and rheobase) did not differ between sexes. These data

suggest that neurons from male mice may be coupled with presynaptic glutamatergic input more efficiently in males than in females, or that the quantal release of glutamate is greater in males than in females, at this age. It was reported previously that nicotinic response amplitude measured in RF (β2) neurons within layer VI of the juvenile mouse mPFC is greater in males than in females[54]. Although we did not observe this sex difference in RF (β2) neurons within layer V at this age, the net charge of nicotinic responses was greater in neurons from male mice due to the slower response decay kinetics in this sex. We observed no sex difference in the α7 or α7/β2 responses from this study.

Pyramidal neurons within layer V of the mPFC provide the primary output signal from this region and project to a wide variety of targets within limbic-cognitive circuits, including the insular cortex, lateral hypothalamus, ventral striatum (nucleus accumbens), dorsal striatum (caudate/putamen), lateral hypothalamus, basolateral amygdala, ventral tegmental area, and brainstem/spinal cord[39,55,56]. It is known that layer V pyramidal neurons located within other cortical regions (e.g., visual, somatosensory, and motor cortex) exhibit distinct physiological and morphological properties depending on their projection targets[23,25,57,58]. It also has been demonstrated previously that layer V pyramidal neuron subtypes located within the auditory cortex having intracortical (intratelencephalic; IT) and subcortical (pyramidal tract; PT) projections are both modulated by β2 nicotinic responses[45]. This differs from our findings in the mPFC, which identify three distinct layer V pyramidal neuron subtypes having distinct projection targets, electrophysiological and morphological properties, and receptor isoform-specific nicotinic responses: IT BF(α7) neurons projecting to the contralateral mPFC, IT BF (α7/β2) neurons projecting to the ipsilateral striatum (nucleus accumbens), and PT RF (β2) neurons projecting to the ipsilateral ventromedial thalamus. Subtypes of IT and PT neurons in dorsal cortical regions show unique activity during, and contributions toward, an auditory decision task, with PT neurons making the greatest contribution[59,60]. While it remains to be determined

whether this finding applies to PT RF (β2) pyramidal neurons located within layer V of the mPFC, the unique electrophysiological properties and nicotinic responses of the pyramidal neuron subtypes identified in our study likely lead them to make distinct contributions toward mPFC-dependent and ACh-supported cognitive tasks.

Methods

Experimental animals

All experiments were performed using CD1-strain mice in accordance with the principles and guidelines of the Canadian Council on Animal Care, and under protocols that were approved by the University of Guelph Animal Care Committee. Pregnant mice were purchased from Charles River Canada (Saint-Constant, Quebec, Canada) and used to establish a local breeding colony. Mice were housed at an ambient temperature of 21-24°C with lights maintained on a 12-hour cycle (lights on at 8:00 pm) and were provided *ad libitum* access to food and water.

Whole-cell electrophysiology in acute brain slices

Male and female mice between postnatal day (P) 15-20 were anesthetized using isoflurane and killed by decapitation. Whole brains were rapidly removed under 4°C oxygenated sucrose artificial cerebrospinal fluid (sACSF) (in mM: 245 sucrose, 10 D-Glucose, 26 $NaHCO_3$, 2 $CaCl_2$, 2 $MgSO_4$, 3 KCl, and 1.25 NaH_2PO_4, pH 7.4). Coronal slices containing the mPFC from approximately Bregma +1.98 mm to +1.34 mm[1] were made at 400 µm thickness using a Leica VT1200 vibrating microtome (Leica Microsystems Inc., Concord, Ontario, Canada). Slices were transferred to a recovery chamber containing oxygenated regular ACSF (in mM; 128 NaCl, 10 D-glucose, 26 NaH_2CO_3, 2 $CaCl_2$, 2 $MgSO_4$, 3 KCl, and 1.25 NaH_2PO_4, pH 7.4) and maintained at 30°C for at least two hours prior to electrophysiology recordings.

Slices were transferred to a recording chamber (Warner Instruments, Hamden, Connecticut, USA), superfused with fresh oxygenated ACSF at room temperature, and visualized using infrared differential interference contrast microscopy. Layer V pyramidal neurons were sampled for recording randomly within layer V of the prelimbic region, based on their location 400-550 µm from the pial surface[2,3], large soma size, pyramidal shape, and prominent apical dendrite projecting toward the pial surface. Whole-cell electrophysiological recordings were conducted using borosilicate glass electrodes having an internal resistance of

3-5 MΩ (Sutter Instrument Company, Novato, California, USA). The electrode solution contained (in mM): 120 K-gluconate, 5 KCl, 2 $MgCl_2$, 4 K_2-ATP, 0.4 Na_2-GTP, 10 Na_2-phosphocreatine, 10 HEPES buffer (pH 7.3). Recordings were made using a Multiclamp 700B amplifier, with signals acquired at 20 kHz and low-pass filtered at 2 kHz using a Digidata 1440A digitizer (Molecular Devices, San Jose, California, USA). The liquid junction potential was corrected at the time of recording.

Measurement of intrinsic electrophysiological properties

Neuron intrinsic electrophysiological properties were first measured in current clamp mode. Resting membrane potential was measured shortly after the whole-cell configuration was achieved with no current injection. Membrane resistance was calculated based on the change in membrane potential from rest in response to 500 ms of -100 pA current. Inter-spike interval (ISI) ratio was used to assess spike frequency adaptation and was calculated as the ratio of durations between the first two action potentials and last two action potentials generated in response to 500 ms of 200 pA current. Sag ratio was calculated as the ratio between the lowest membrane potential and the steady-state membrane potential generated in response to 500 ms of -100 pA current. Rheobase was measured by injecting 500 ms of positive current that increased in magnitude by 5 pA with each step until a single action potential was elicited. Action potential amplitude was measured at rheobase as the difference between the threshold potential and the peak potential. Postburst afterhyperpolarization (AHP) responses were measured as the difference between the resting membrane potential and the lowest membrane potential attained after injection of 1, 2, 4, 8, 16, and 32 current pulses (2 ms, 2-nA, at 50 Hz). Input/output curves were generated by measuring the number of action potentials elicited in response to 500 ms positive current steps that increased in 50 pA increments.

Measurement of spontaneous excitatory postsynaptic currents

Spontaneous EPSCs were recorded in voltage-clamp mode at a holding potential of −75 mV for a 30s period. Tracings were analyzed offline using a template search in Clampfit software. Events that were <5 or >100 pA were not included in the analysis. EPSC frequency, amplitude, and net charge were measured.

Measurement of postsynaptic nicotinic currents

Postsynaptic nicotinic currents were measured in voltage-clamp mode at -75 mV in the presence of 200 nM atropine to block muscarinic receptors. 1 mM ACh was prepared in ACSF within a borosilicate glass application pipette having a resistance of 3-5 MΩ and pressure applied at 10 psi for 100 ms using a Picospritzer II (General Valve, Fairfield, New Jersey, USA). The application pipette was positioned 20-50 µm from the soma, perpendicular to the pial surface. Some initial experiments were performed in the presence of 10 nM MLA citrate (Tocris / Bio-Techne Canada, Toronto, Ontario, Canada) and/or 3 µM DHβE hydrobromide (Tocris) to determine the contribution of α7 and β2 subunit-containing nAChRs, respectively (Fig. 1). Pressure application of ACSF alone did not alter the holding currents in these experiments.

Nicotinic currents were measured using a custom-written program in MATLAB (MathWorks, Natick, Maine, USA). Current amplitude, net charge, response time, rise and decay kinetics were used to characterized nicotinic currents mediated by α7, α7/β2, and β2 responses (Fig. 2). Rise and decay kinetics were analyzed separately using nonlinear least-squares curve fitting via an eight-term Fourier series equation. Nicotinic currents mediated by α7 and β2 nAChRs were distinguishable based on rise and decay kinetics, which were significantly more rapid for α7 nAChRs than for β2 nAChRs. In the subset of neurons that exhibited nicotinic currents mediated by α7/β2 nAChRs, the second decay tau ($D\tau_2$) threshold of 930 ms was used to distinguish between currents mediated by α7 and α7/β2 nAChRs.

Correlation matrix and principal component analysis

A total of seven measures of intrinsic electrophysiological properties, three measures of EPSCs, and five measures of nicotinic currents were used to generate a correlation matrix and perform principal component analysis within each sex (Fig. 5). The Pearson correlation coefficient and its associated *p* value were calculated for each possible pair of measures for all neurons irrespective of their nicotinic current responses. Principal component analysis was used to visualize the distribution of neuron types (categorized based on nicotinic responses) in multidimensional space. The Kaiser-Gutman criterion was used to decide the initial number of PCs. Only PCs with an eigenvalue equal to or greater than one were selected for subsequent analysis. The selection of significant PCs was confirmed using a scree plot of all PCs. Significant PCs were then used to produce a three-dimension scatterplot matrix.

Visualization and measurement of neuron morphology

During electrophysiological recordings, a subset of neurons exhibiting each type of nicotinic response were labelled with 0.3% (wt/vol) biocytin (Tocris) in the electrode solution. Brain slices were fixed in 4% (wt/vol) paraformaldehyde in 100 mM phosphate buffer (pH 7.5) for up to 3 weeks at 4°C. Slices were washed in Tris-buffered saline (TBS, 100 mM Tris and 150 mM NaCl, pH 7.5) 3 x 10 min at room temperature and incubated with 0.5% (vol/vol) H_2O_2 and 0.25% (vol/vol) Triton X-100 in TBS for 15 min at room temperature. Slices were washed in TBS 3 x 10 min at room temperature and incubated with 0.25% (vol/vol) VECTASTAIN Elite reagent A (avidin), 0.25% (vol/vol) VECTASTAIN Elite reagent B (biotinylated horseradish peroxidase), and 0.25% (vol/vol) Triton X-100 in TBS for 24 hours at room temperature (Vector Labs, Burlingame, California, USA). Slices were washed in TBS 3 x 10 min at room temperature and incubated with 0.05% (wt/vol) 3,3′-diaminobenzidine tetrahydrochloride hydrate (DAB), 0.04% (wt/vol) nickel chloride hexahydrate, and 0.25% (vol/vol) Triton X-100 in TBS for 5 min at room temperature. Slices were then incubated in this same DAB/nickel/Triton X-100 solution that also contained 0.001% (vol/vol) H_2O_2 for 15 minutes at room temperature. The reaction was stopped

by washing slices 3 x 10 min in TBS at room temperature, after which slices were mounted onto microscope slides and allowed to air dry. Slides were dehydrated through ethanol gradients and coverslipped using Permount (Fisher Scientific, Ottawa, Ontario, Canada).

Individuals involved in neuron imaging and analysis were blinded to the experimental groups. Brightfield image stacks containing labelled neurons were captured using an Olympus BX53 upright microscope equipped with an Olympus UPlanSApo 30x / 1.05 N.A. silicone-immersion objective (Olympus Canada Inc., Richmond Hill, Ontario, Canada), which was controlled by Neurolucida software (MBF Bioscience, Williston, Vermont, USA). Labelled pyramidal neurons were reconstructed and measured only if they contained one prominent apical dendrite that projected toward the pial surface and all dendrites were fully contained within the slice. Neurons were reconstructed in three dimensions using Neuromantic software[4] and their morphology was measured using Neurolucida Explorer software (MBF Bioscience). Modified Sholl analyses were conducted separately on apical and basal dendrites, in which the length, diameter, and volume of dendrites were measured between concentric spheres radiating from the soma in 25 µm increments.

Retrograde labelling

Male and female mice underwent retrograde labelling surgery on P18. Three-to-four mice were used for each sex and labelling region. Carprofen was administered s.c. to the back at 20 mg/kg one hour before surgery. Mice were anaesthetised using isoflourane and placed in a stereotaxic apparatus (David Kopf Instruments, Tujunga, California, USA). The scalp was shaved and anesthetized with the s.c. administration of 50 µL of a local anesthetic cocktail containing 0.67% lidocaine and 0.17% bupivacaine, made from stock solutions in a volumetric ratio of 3:6:9 lidocaine:bupivacaine:saline. The scalp was cut along the midline and a small hole was drilled in the skull above the labelling region of interest. Relative to bregma, coordinates for each labeling region were: mPFC: AP: 1.8 mm, ML: -0.35 or 0.35 mm, DV: -2.6 mm, nucleus accumbens: AP:

1.1 mm, ML: -2.6 or 2.6 mm, DV -3.9 mm; 15° angle from vertical, and ventromedial thalamus: AP: -1.3 mm, ML: -0.75 or 0.75 mm, DV: -4.2 mm. A custom microinjector delivered 0.3 µL of rhodamine-labelled RetroBeads (0.5x dilution; LumaFluor Inc., Durham, North Carolina, USA) into the labelling region at a rate of 1 µL/min using infusion pump (model PHD 2000; Harvard Apparatus, Holliston, Maine, USA). Microinjectors were left in place for an additional 10 minutes, after which they were removed slowly and exposed skull was covered with dental cement. Mice were returned to their home cage for at least 48 h and killed for electrophysiology experiments at P20-21 as described above. Coronal brain sections containing the mPFC were visualized using epifluorescence and retrograde-labelled pyramidal neurons were assessed for physiology and morphology using whole-cell electrophysiology with biocytin labelling as described above.

Confocal Microscopy

After recording of retrograde-labelled neurons, brain slices were fixed in 4% (wt/vol) paraformaldehyde in 100 mM phosphate buffer at overnight at 4°C. Slices were washed in TBS 3 x 10 min at room temperature and incubated in blocking buffer comprising 10% (wt/vol) bovine serum albumin (BSA) and 0.25% (vol/vol) Triton X-100 in TBS for two hours at room temperature. Slices were washed in TBS 3 x 10 min at room temperature and incubated in a solution comprising 3% (wt/vol) BSA, 0.25% (vol/vol) Triton X-100, and 4 µg/mL streptavidin conjugated with Alex Fluor-488 (Fisher Scientific) in TBS overnight at 4°C. Slices were washed in TBS 3 x 10 min at room temperature and incubated with 1 µg/mL 4',6-diamidino-2-phenylindole (DAPI) in TBS for two hours at room temperature. Slices were washed in TBS 3 x 10 min at room temperature and mounted onto microscope slides and coverslipped using an aqueous mounting medium.

Processed slices were imaged using an Olympus Fluoview FV1200 laser-scanning confocal system connected with an inverted Olympus IX83 microscope and controlled using Olympus Fluoview software (FV10-ASW version 4.0; Olympus). A helium neon laser tuned to

405 nm (DAPI), 488 nm (retrograde labelled neuron), or 543 nm (RetroBeads) and an Olympus UPlanSApo 30X, 1.05 NA silicone oil-immersion objective were used to acquire three-channel image stacks which, when stitched together in three dimensions, contained entire retrograde labelled neurons.

Statistical Analysis

Electrophysiological recordings were analyzed using Clampfit software (version 10, Molecular Devices) and custom scripts written for MATLAB software (version 9.7, MathWorks). Statistical analyses were conducted using GraphPad Prism software (version 9, GraphPad Software). Data were analysed using the Chi-square test, two-way ANOVA with the Bonferroni *post hoc* correction, or Pearson correlation, as indicated. Data are presented for individual neurons and as group means ± 1 SEM. For all figures, statistical significance is indicated as $*p < 0.05$, $**p < 0.01$, $***p < 0.001$, and $****p < 0.0001$. The sample size for each group is listed in the respective figure legend.

Data Availability

All data that were generated and presented in this manuscript are available from the corresponding author (C.D.C.B.) upon reasonable request.

References

1 Granon, S., Poucet, B., Thinus-Blanc, C., Changeux, J. P. & Vidal, C. Nicotinic and muscarinic receptors in the rat prefrontal cortex: differential roles in working memory, response selection and effortful processing. *Psychopharmacology (Berl)* **119**, 139-144 (1995).

2 Parikh, V., Kozak, R., Martinez, V. & Sarter, M. Prefrontal acetylcholine release controls cue detection on multiple timescales. *Neuron* **56**, 141-154 (2007).

3 Parikh, V. & Sarter, M. Cholinergic mediation of attention: contributions of phasic and tonic increases in prefrontal cholinergic activity. *Ann.N.Y.Acad.Sci.* **1129**, 225-235 (2008).

4 Bailey, C. D., De Biasi, M., Fletcher, P. J. & Lambe, E. K. The nicotinic acetylcholine receptor α5 subunit plays a key role in attention circuitry and accuracy. *The Journal of neuroscience : the official journal of the Society for Neuroscience* **30**, 9241-9252 (2010).

5 Guillem, K. *et al.* Nicotinic acetylcholine receptor β2 subunits in the medial prefrontal cortex control attention. *Science* **333**, 888-891 (2011).

6 Disney, A. A. & Higley, M. J. Diverse Spatiotemporal Scales of Cholinergic Signaling in the Neocortex. *The Journal of neuroscience : the official journal of the Society for Neuroscience* **40**, 720-725 (2020).

7 Sarter, M. & Lustig, C. Forebrain Cholinergic Signaling: Wired and Phasic, Not Tonic, and Causing Behavior. *The Journal of neuroscience : the official journal of the Society for Neuroscience* **40**, 712-719 (2020).

8 Passetti, F., Dalley, J. W., O'Connell, M. T., Everitt, B. J. & Robbins, T. W. Increased acetylcholine release in the rat medial prefrontal cortex during performance of a visual attentional task. *Eur.J.Neurosci.* **12**, 3051-3058 (2000).

9 Dalley, J. W. *et al.* Distinct changes in cortical acetylcholine and noradrenaline efflux during contingent and noncontingent performance of a visual attentional task. *The Journal of neuroscience : the official journal of the Society for Neuroscience* **21**, 4908-4914 (2001).

10 Hironaka, N., Tanaka, K., Izaki, Y., Hori, K. & Nomura, M. Memory-related acetylcholine efflux from rat prefrontal cortex and hippocampus: a microdialysis study. *Brain research* **901**, 143-150 (2001).

11 Hoyle, E., Genn, R. F., Fernandes, C. & Stolerman, I. P. Impaired performance of alpha7 nicotinic receptor knockout mice in the five-choice serial reaction time task. *Psychopharmacology (Berl)* **189**, 211-223 (2006).

12 Pastor, V. *et al.* Prefrontal cortex nicotinic receptor inhibition by methyllycaconitine impaired cocaine-associated memory acquisition and retrieval. *Behavioural brain research* **406**, 113212 (2021).

13 Patel, A. V. *et al.* Developmental age and biological sex influence muscarinic receptor function and neuron morphology within layer VI of the medial prefrontal cortex. *Cereb Cortex* **32**, 3137-3158 (2022).

14 Couey, J. J. *et al.* Distributed network actions by nicotine increase the threshold for spike-timing-dependent plasticity in prefrontal cortex. *Neuron* **54**, 73-87 (2007).

15 Poorthuis, R. B. *et al.* Layer-specific modulation of the prefrontal cortex by nicotinic acetylcholine receptors. *Cereb Cortex* **23**, 148-161 (2013).

16 Zolles, G., Wagner, E., Lampert, A. & Sutor, B. Functional expression of nicotinic acetylcholine receptors in rat neocortical layer 5 pyramidal cells. *Cereb Cortex* **19**, 1079-1091 (2009).

17 van Aerde, K. I. & Feldmeyer, D. Morphological and physiological characterization of pyramidal neuron subtypes in rat medial prefrontal cortex. *Cereb Cortex* **25**, 788-805 (2015).

18 Hedrick, T. & Waters, J. Spiking patterns of neocortical L5 pyramidal neurons in vitro change with temperature. *Front Cell Neurosci* **5**, 1 (2011).

19 McCormick, D. A., Connors, B. W., Lighthall, J. W. & Prince, D. A. Comparative electrophysiology of pyramidal and sparsely spiny stellate neurons of the neocortex. *Journal of neurophysiology* **54**, 782-806 (1985).

20 Franceschetti, S., Sancini, G., Panzica, F., Radici, C. & Avanzini, G. Postnatal differentiation of firing properties and morphological characteristics in layer V pyramidal neurons of the sensorimotor cortex. *Neuroscience* **83**, 1013-1024 (1998)

21 Chagnac-Amitai, Y., Luhmann, H. J. & Prince, D. A. Burst generating and regular spiking layer 5 pyramidal neurons of rat neocortex have different morphological features. *The Journal of comparative neurology* **296**, 598-613 (1990).

22 Agmon, A. & Connors, B. W. Correlation between intrinsic firing patterns and thalamocortical synaptic responses of neurons in mouse barrel cortex. *The Journal of neuroscience : the official journal of the Society for Neuroscience* **12**, 319-329 (1992).

23 Molnar, Z. & Cheung, A. F. Towards the classification of subpopulations of layer V pyramidal projection neurons. *Neurosci Res* **55**, 105-115 (2006).

24 Mason, A. & Larkman, A. Correlations between morphology and electrophysiology of pyramidal neurons in slices of rat visual cortex. II. Electrophysiology. *The Journal of neuroscience : the official journal of the Society for Neuroscience* **10**, 1415-1428 (1990).

25 Hattox, A. M. & Nelson, S. B. Layer V neurons in mouse cortex projecting to different targets have distinct physiological properties. *Journal of neurophysiology* **98**, 3330-3340 (2007).

26 Kim, E. J., Juavinett, A. L., Kyubwa, E. M., Jacobs, M. W. & Callaway, E. M. Three Types of Cortical Layer 5 Neurons That Differ in Brain-wide Connectivity and Function. *Neuron* **88**, 1253-1267 (2015).

27 Graves, A. R. *et al.* Hippocampal pyramidal neurons comprise two distinct cell types that are countermodulated by metabotropic receptors. *Neuron* **76**, 776-789 (2012).

28 Wu, J. *et al.* Heteromeric α7β2 Nicotinic Acetylcholine Receptors in the Brain. *Trends Pharmacol Sci* **37**, 562-574 (2016).

29 Chung, B. Y. T. & Bailey, C. D. C. Similar nicotinic excitability responses across the developing hippocampal formation are regulated by small-conductance calcium-activated potassium channels. *Journal of neurophysiology* **119**, 1707-1722 (2018).

30 Hay, Y. A., Lambolez, B. & Tricoire, L. Nicotinic Transmission onto Layer 6 Cortical Neurons Relies on Synaptic Activation of Non-α7 Receptors. *Cereb Cortex* **26**, 2549-2562 (2016).

31 Thomsen, M. S. *et al.* α7 and β2 Nicotinic Acetylcholine Receptor Subunits Form Heteromeric Receptor Complexes that Are Expressed in the Human Cortex and Display Distinct Pharmacological Properties. *PloS one* **10**, e0130572 (2015).

32 Rayi, P. R. & Kaphzan, H. Electrophysiological Characterization of Regular and Burst Firing Pyramidal Neurons of the Dorsal Subiculum in an Angelman Syndrome Mouse Model. *Front Cell Neurosci* **15**, 670998 (2021).

33 Degenetais, E., Thierry, A. M., Glowinski, J. & Gioanni, Y. Electrophysiological properties of pyramidal neurons in the rat prefrontal cortex: an in vivo intracellular recording study. *Cereb Cortex* **12**, 1-16 (2002).

34 Lambe, E. K., Picciotto, M. R. & Aghajanian, G. K. Nicotine induces glutamate release from thalamocortical terminals in prefrontal cortex. *Neuropsychopharmacology* **28**, 216-225 (2003).

35 Kroon, T., van Hugte, E., van Linge, L., Mansvelder, H. D. & Meredith, R. M. Early postnatal development of pyramidal neurons across layers of the mouse medial prefrontal cortex. *Sci Rep* **9**, 5037 (2019).

36 Bailey, C. D., Alves, N. C., Nashmi, R., De Biasi, M. & Lambe, E. K. Nicotinic α5 subunits drive developmental changes in the activation and morphology of prefrontal cortex layer VI neurons. *Biological psychiatry* **71**, 120-128 (2012).

37 Baker, A. *et al.* Specialized Subpopulations of Deep-Layer Pyramidal Neurons in the Neocortex: Bridging Cellular Properties to Functional Consequences. *The Journal of neuroscience : the official journal of the Society for Neuroscience* **38**, 5441-5455 (2018).

38 Hoover, W. B. & Vertes, R. P. Anatomical analysis of afferent projections to the medial prefrontal cortex in the rat. *Brain Struct Funct* **212**, 149-179 (2007).

39 Gabbott, P. L., Warner, T. A., Jays, P. R., Salway, P. & Busby, S. J. Prefrontal cortex in the rat: projections to subcortical autonomic, motor, and limbic centers. *J.Comp Neurol.* **492**, 145-177 (2005).

40 Verhoog, M. B. *et al.* Layer-specific cholinergic control of human and mouse cortical synaptic plasticity. *Nat Commun* **7**, 12826 (2016).

41 Aracri, P., Meneghini, S., Coatti, A., Amadeo, A. & Becchetti, A. $\alpha4\beta2$* nicotinic receptors stimulate GABA release onto fast-spiking cells in layer V of mouse prefrontal (Fr2) cortex. *Neuroscience* **340**, 48-61 (2017).

42 Bloem, B., Poorthuis, R. B. & Mansvelder, H. D. Cholinergic modulation of the medial prefrontal cortex: the role of nicotinic receptors in attention and regulation of neuronal activity. *Front Neural Circuits* **8**, 17 (2014).

43 Komal, P., Gudavicius, G., Nelson, C. J. & Nashmi, R. T-cell receptor activation decreases excitability of cortical interneurons by inhibiting $\alpha7$ nicotinic receptors. *The Journal of neuroscience : the official journal of the Society for Neuroscience* **34**, 22-35 (2014)

44 Obermayer, J. *et al.* Prefrontal cortical ChAT-VIP interneurons provide local excitation by cholinergic synaptic transmission and control attention. *Nat Commun* **10**, 5280 (2019).

45 Joshi, A., Kalappa, B. I., Anderson, C. T. & Tzounopoulos, T. Cell-Specific Cholinergic Modulation of Excitability of Layer 5B Principal Neurons in Mouse Auditory Cortex. *The Journal of neuroscience : the official journal of the Society for Neuroscience* **36**, 8487-8499 (2016).

46 Womelsdorf, T., Ardid, S., Everling, S. & Valiante, T. A. Burst firing synchronizes prefrontal and anterior cingulate cortex during attentional control. *Curr Biol* **24**, 2613-2621 (2014).

47 Voloh, B. & Womelsdorf, T. Cell-Type Specific Burst Firing Interacts with Theta and Beta Activity in Prefrontal Cortex During Attention States. *Cereb Cortex* **28**, 4348-4364 (2018).

48 Schubert, D., Kotter, R., Luhmann, H. J. & Staiger, J. F. Morphology, electrophysiology and functional input connectivity of pyramidal neurons characterizes a genuine layer va in the primary somatosensory cortex. *Cereb Cortex* **16**, 223-236 (2006).

49 Jiang, S. *et al.* Anatomically revealed morphological patterns of pyramidal neurons in layer 5 of the motor cortex. *Sci Rep* **10**, 7916 (2020).

50 Ramaswamy, S. & Markram, H. Anatomy and physiology of the thick-tufted layer 5 pyramidal neuron. *Front Cell Neurosci* **9**, 233 (2015).

51 Yang, C. R., Seamans, J. K. & Gorelova, N. Electrophysiological and morphological properties of layers V-VI principal pyramidal cells in rat prefrontal cortex in vitro. *The Journal of neuroscience : the official journal of the Society for Neuroscience* **16**, 1904-1921 (1996).

52 Schwindt, P. & Crill, W. Mechanisms underlying burst and regular spiking evoked by dendritic depolarization in layer 5 cortical pyramidal neurons. *Journal of neurophysiology* **81**, 1341-1354 (1999).

53 Works, S. J., Wilson, R. E. & Wellman, C. L. Age-dependent effect of cholinergic lesion on dendritic morphology in rat frontal cortex. *Neurobiology of aging* **25**, 963-974 (2004).

54 Alves, N. C., Bailey, C. D., Nashmi, R. & Lambe, E. K. Developmental sex differences in nicotinic currents of prefrontal layer VI neurons in mice and rats. *PLoS.One.* **5**, e9261 (2010).

55 Vertes, R. P. Differential projections of the infralimbic and prelimbic cortex in the rat. *Synapse* **51**, 32-58 (2004).

56 Ding, D. C., Gabbott, P. L. & Totterdell, S. Differences in the laminar origin of projections from the medial prefrontal cortex to the nucleus accumbens shell and core regions in the rat. *Brain research* **917**, 81-89 (2001).

57 Hallman, L. E., Schofield, B. R. & Lin, C. S. Dendritic morphology and axon collaterals of corticotectal, corticopontine, and callosal neurons in layer V of primary visual cortex of the hooded rat. *The Journal of comparative neurology* **272**, 149-160 (1988).

58 Gao, W. J. & Zheng, Z. H. Target-specific differences in somatodendritic morphology of layer V pyramidal neurons in rat motor cortex. *The Journal of comparative neurology* **476**, 174-185 (2004).

59 Musall, S. *et al.* Pyramidal cell types drive functionally distinct cortical activity patterns during decision-making. *Nat Neurosci* **26**, 495-505 (2023).

60 Mohan, H. *et al.* Cortical glutamatergic projection neuron types contribute to distinct functional subnetworks. *Nat Neurosci* **26**, 481-494 (2023)

Acknowledgements

Funding for this work was provided by Discovery Grants from the Natural Sciences and Engineering Council of Canada (NSERC) to C.D.C.B. (RGPIN-2019-04989) and E.C. (RGPIN-2018-04699), and by a Canada Foundation for Innovation (CFI) grant to C.D.C.B. (30381). We thank Dr. Matthew Vickaryous at the University of Guelph for the use of a fluorescence filter cube.

Author contributions

A.V.P. and C.D.C.B. conceived and designed the study. A.V.P., A.N., and P.P. performed experiments. E.C. provided resources and supervised experiments. C.D.C.B. supervised the entire study. A.V.P. and C.D.C.B. analyzed all results and wrote the manuscript. All authors have reviewed and approved the final manuscript.

Competing interests

The authors declare no competing interests.

Figure legends

Fig. 1 Prefrontal layer V pyramidal neuron subtypes have distinct nicotinic responses

Pyramidal neurons were sampled randomly from layer V of the mouse prelimbic cortex and recorded for intrinsic electrophysiological properties and nicotinic acetylcholine responses. Three distinct neuron subtypes were identified based on nicotinic responses. **a** The most common neuron subtype exhibited an initial burst-firing pattern of action potentials in response to the injection of 200 pA positive current (**a_1**). Its nicotinic response to 100 ms application of 1 mM ACh (indicated by the red arrowhead in **a_2**) had fast rise and decay kinetics characteristic of homomeric α7 nAChRs, which was confirmed by the lack of effect of 3 μM DHβE (**a_3**) and the complete elimination by 10 nM MLA (**a_4**). A second neuron subtype also exhibited a burst-firing pattern of action potentials (**b_1**) but its nicotinic response contained both fast and slow components (**b_2**). Fast components were eliminated by 10 nM MLA (**b_3**) and the remaining slow components were eliminated by 3 μM DHβE (**b_4**), which suggests the presence of both homomeric α7 and heteromeric β2 nAChRs. A third neuron subtype exhibited a regular-firing pattern of action potentials (**c_1**) and nicotinic responses that consistently had slow rise and decay kinetics characteristic of heteromeric β2 nAChRs (**c_2**). This was confirmed by the lack of effect of 10 nM MLA (**c_3**) and the complete elimination by 3 μM DHβE (**c_4**). **d** Pie charts show the proportion of sampled neurons that belong to each subtype for male and female mice. These proportions were not statistically different between sexes (Chi-square test, X^2 (2, n = 120) = 0.55, p = 0.76).

Fig. 2 Characterization of nicotinic responses for pyramidal neuron subtypes

A detailed analysis of inward current response kinetics was performed for the three pharmacologically-identified nicotinic responses from the three pyramidal neuron subtypes. Peak response amplitude (**a**) and net charge (**b**) showed no sex difference (two-way ANOVA,

each $p \geq 0.2$) but did show opposite effects of response type (each $p < 0.0001$). The time to peak (**c**) and rise tau (**d**) showed no sex difference (each $p \geq 0.4$), but were both affected by response type (each $p \leq 0.0001$) with β2 nAChR responses exhibiting the slowest response onset. The first decay tau (**e**) and second decay tau (**f**) showed no sex difference (each $p \geq 0.4$), but were both affected by response type (each $p \leq 0.0001$) with β2 nAChR responses exhibiting the slowest response decay amongst the response types. Of note, the second decay tau was significantly different between each the α7, α7/β2, and β2 nAChR responses within each sex (Bonferroni *post hoc* correction, each comparison $p < 0.0001$). **g** One typical tracing is shown for each nicotinic response type with the solid area under the curve representing the net charge conducted. **h** The same typical tracings are shown with an eight-term Fourier series curve fitting to determine rise and decay kinetics. The rise tau (R_τ) is indicated by the green cross within each expanded box, while the first decay tau (D_{τ_1}) and second decay tau (D_{τ_2}) are indicated by green crosses within the full tracings. All data are shown for individual neurons and as mean +/- 1 SEM. Sample sizes for males are: burst-firing (α7) = 29; burst-firing (α7/β2) = 13; regular-firing (β2) = 15, and for females are: burst-firing (α7) = 35; burst-firing (α7/β2) = 15; regular-firing (β2) = 13. Significance levels for Bonferroni *post hoc* corrections within each sex are *$p < 0.05$, **$p < 0.01$, ***$p < 0.001$, and ****$p < 0.0001$.

Fig. 3 Characterization of intrinsic electrophysiological properties for pyramidal neuron subtypes

Membrane resistance (**a**) showed no sex difference (two-way ANOVA, $p = 0.4$), but was affected by neuron subtype ($p < 0.0001$) with resistance being greatest in regular-firing (β2) neurons (Bonferroni *post hoc* correction, all $p \leq 0.001$). The same scenario was observed for interspike interval ratio (**b**), which showed no sex difference ($p = 0.09$), but was affected by neuron subtype ($p < 0.0001$) with the interspike interval ratio being greatest in regular-firing (β2)

neurons (all $p \leq 0.001$). Rheobase (**c**) showed a sex difference ($p = 0.02$) and was affected by neuron subtype ($p = 0.008$). Sag ratio (**d**) showed no sex difference ($p = 0.09$) and was not affected by neuron subtype ($p = 0.07$). Input / output curves showed similar effects of neuron subtype within males (**e**) and females (**f**), where two-way ANOVA identified no overall effect of neuron subtype (males: $p = 0.8$; females: $p = 0.2$) but a significant interaction between effects of neuron subtype and the amount of current injected ($p < 0.0001$ for each sex). Firing output was different in regular-firing (β2) neurons than in the other neuron subtypes where indicated (each $p < 0.05$). A similar scenario was observed for AHP amplitude in males (**g**) and females (**h**), with no overall effect of neuron subtype (males: $p = 0.1$; females $p = 0.7$) but a significant interaction between effects of neuron subtype and the number of current pulses (males: $p < 0.0001$; females: $p = 0.02$). AHP amplitude was lower in regular-firing (β2) neurons than in burst-firing (α7/β2) neurons for males only (as indicated; each $p < 0.05$). All data are shown for individual neurons and/or as mean +/- 1 SEM. Sample sizes for males are: burst-firing (α7) = 29; burst-firing (α7/β2) = 13; regular-firing (β2) = 15, and for females are: burst-firing (α7) = 35; burst-firing (α7/β2) = 15; regular-firing (β2) n = 13. Significance levels for Bonferroni *post hoc* corrections within each sex are *$p < 0.05$, **$p < 0.01$, ***$p < 0.001$, and ****$p < 0.0001$.

Fig. 4 Characterization of spontaneous presynaptic input to pyramidal neuron subtypes

Spontaneous EPSC frequency (**a**) showed no sex difference (two-way ANOVA, $p = 0.6$), but was affected by neuron subtype ($p < 0.0001$) with frequency being lowest in regular-firing (β2) neurons (Bonferroni *post hoc* correction, $p < 0.01$ or $p < 0.001$ as indicated). EPSC amplitude (**b**) showed a sex difference ($p < 0.0001$) and an effect of neuron subtype ($p < 0.0001$), with amplitude being lowest in regular-firing (β2) neurons ($p < 0.01$ as indicated). Similarly, EPSC net charge showed a sex difference ($p < 0.0001$) and an effect of neuron subtype ($p < 0.0001$), with net charge being lowest in regular-firing (β2) neurons ($p < 0.05$, $p < 0.01$, or $p < 0.0001$ as

indicated). Typical voltage-clamp traces with EPSCs are shown for one pyramidal neuron from each subtype in males (**d**) and females (**e**). The average of 200 representative EPSCs is shown for pyramidal neurons from each subtype in males (**f**) and females (**g**). All data are shown for individual neurons and as mean +/- 1 SEM. Sample sizes for males are: burst-firing ($\alpha7$) = 29; burst-firing ($\alpha7/\beta2$) = 13; regular-firing ($\beta2$) = 15, and for females are: burst-firing ($\alpha7$) = 35; burst-firing ($\alpha7/\beta2$) = 15; regular-firing ($\beta2$) n = 13. Significance levels for Bonferroni *post hoc* corrections within each sex are *$p < 0.05$, **$p < 0.01$, ***$p < 0.001$, and ****$p < 0.0001$.

Fig. 5 Correlation and principal component analyses for electrophysiological properties of pyramidal neuron subtypes

a Correlation matrix comprising eight intrinsic electrophysiological properties, six measures of nicotinic current responses, and three measures of spontaneous EPSCs. Male data is presented on the lower-left and female data is presented on the upper-right. For each comparison, the corresponding cell contains the Pearson correlation coefficient, a graphical representation of the correlation analysis, and the line of best fit. Cells with significant positive correlations are shown in green and cells with significant negative correlations are shown in red (each $p < 0.05$). **b** Principal component analysis included all measures from the correlation matrix. Three-dimension plots are shown for the first three principal components (PCs) that account for 65.9% of variability in males and 60.0% of variability in females. In both sexes, regular-firing ($\beta2$) neurons form an unambiguous cluster separate from the other two burst-firing neuron subtypes. Sample sizes for males are: burst-firing ($\alpha7$) = 29; burst-firing ($\alpha7/\beta2$) = 13; regular-firing ($\beta2$) = 15, and for females are: burst-firing ($\alpha7$) = 35; burst-firing ($\alpha7/\beta2$) = 15; regular-firing ($\beta2$) n = 13.

Fig. 6 Dendrite morphology of pyramidal neuron subtypes

Sholl plots are shown for dendrite length, diameter, and volume as a function of distance from neuron soma. Data are shown for males on the left side of the figure and for females on the right side of the figure. For each plot, apical dendrite data is oriented to the right of zero, and basal dendrite data is oriented to the left of zero, with zero indicating the location of the soma. Apical dendrite length showed an effect of neuron subtype for both males (**a**) and females (**b**) (two-way ANOVA, each $p < 0.0001$). Burst-firing ($\alpha7$) neurons showed the lowest apical length in males (Bonferroni *post hoc* correction, $p \leq 0.05$) and the greatest apical length in females ($p < 0.0001$). Basal dendrite length showed an effect of neuron subtype in both sexes ($p \leq 0.001$) with the lowest basal length in regular-firing ($\beta2$) neurons ($p \leq 0.05$). Apical dendrite diameter showed an effect of neuron subtype in males (**c**) and females (**d**) (each $p < 0.0001$) whereas basal dendrite diameter showed an effect of neuron subtype in males only ($p < 0.0001$). Apical dendrite volume showed an effect of neuron subtype for both males (**e**) and females (**f**) (each $p < 0.0001$). Burst-firing ($\alpha7/\beta2$) neurons showed the greatest apical dendrite volume in males ($p \leq 0.001$) whereas burst-firing ($\alpha7$) neurons showed the greatest apical dendrite volume in females ($p < 0.0001$). Basal dendrite volume showed an effect of neuron subtype in both sexes ($p \leq 0.0001$) with the lowest basal dendrite volume in regular-firing ($\beta2$) neurons ($p \leq 0.001$). Typical traces of reconstructed pyramidal neurons are shown for males (**g**) and females (**h**) below the Sholl plots for each sex. The scale bar represents 500 μm.

Fig. 7 Sex differences in the morphology of pyramidal neuron subtypes

Sholl plots are shown comparing male and female dendrite volume for each of the pyramidal neuron subtypes. For each plot, apical dendrite data is oriented to the right of zero, and basal dendrite data is oriented to the left of zero, with zero indicating the location of the soma. **a** In burst-firing ($\alpha7$) neurons, apical dendrite volume showed a sex difference (two-way ANOVA, *p*

<0.0001) that depended on the distance from the soma (interaction effect, $p = 0.005$). Apical dendrites from females had a greater volume than those from males (Bonferroni *post hoc* correction, $p < 0.05$ as indicated). Basal dendrite volume also showed a sex difference ($p = 0.02$) that depended on the distance from the soma ($p < 0.0001$). **b** In burst-firing ($\alpha7/\beta2$) neurons, there was no sex difference for apical dendrite volume ($p = 0.06$) or for basal dendrite volume ($p = 0.9$). **c** In regular-firing ($\beta2$) neurons, both apical dendrite volume ($p = 0.03$) and basal dendrite volume ($p = 0.0007$) showed a significant sex difference with no dependence on distance from the soma (both $p = 0.6$). Basal dendrite volume was greater in females, as indicated. Typical traces of reconstructed neurons from each sex are shown below each Sholl plot. The scale bars represent 500 μm. All data are shown as mean +/- 1 SEM. *$p < 0.05$ for a significant sex difference following Bonferroni *post hoc* corrections.

Fig. 8 Retrograde labelling of pyramidal neuron subtypes

Prefrontal layer V pyramidal neurons were recorded after intracranial injection of retrograde tracer into the (**a**) contralateral mPFC, (**b**) ipsilateral nucleus accumbens, or (**c**) ipsilateral ventromedial thalamus. For each injection region, coronal diagrams relative to bregma show the injection site in red. Representative photomicrographs of the mPFC show DAPI-stained nuclei (blue), retrograde tracer (red), and layer V pyramidal neurons containing the retrograde tracer that were recorded for electrophysiology and filled with biocytin (green). For the contralateral mPFC, all retrograde-labelled neurons that were recorded showed a burst-firing response to 200 pA of positive current and an $\alpha7$ nicotinic response to 1 mM ACh (indicated by the red arrowhead). No other nicotinic response was observed. For the ipsilateral nucleus accumbens, all retrograde-labelled neurons that were recorded showed a burst-firing response to 200 pA of positive current and an $\alpha7/\beta2$ nicotinic response to 1 mM ACh. For the ipsilateral ventromedial thalamus, all retrograde-labelled neurons that were recorded showed a regular-firing response

to 200 pA of positive current and a β2 nicotinic response to 1 mM ACh. The contingency table presented for each injection region shows the proportion of recorded neurons that showed each subtype of nicotinic response. Scale bars on the photomicrographs represent 100 μm.

Fig. 9 Graphical summary of nicotinic receptor localization within the prefrontal cortex

Based on previous literature and the findings from this current study, α7 and β2 subunit-containing nAChRs are expressed at distinct sites within the rodent medial prefrontal cortex. Pyramidal neurons (P) in layers II/III do not appear to express nAChRs. Pyramidal neurons in layer V comprise three subtypes identified in this current study that express α7 and/or β2 nAChRs. Pyramidal neurons in layer VI express β2 nAChRs only. Interneurons in layers I, II/III, and V express α7 and/or β2 nAChRs, whereas interneurons in layer VI express β2 nAChRs only. Glutamatergic inputs from the mediodorsal thalamus to layer V pyramidal neurons also express β2 nAChRs. Glutamatergic inputs to the mPFC are shown in blue and outputs to specified projection targets are shown in green. mPFC, medial prefrontal cortex; MDT, mediodorsal thalamus; VMT, ventrolateral thalamus; NAc, nucleus accumbens.

Figure 1

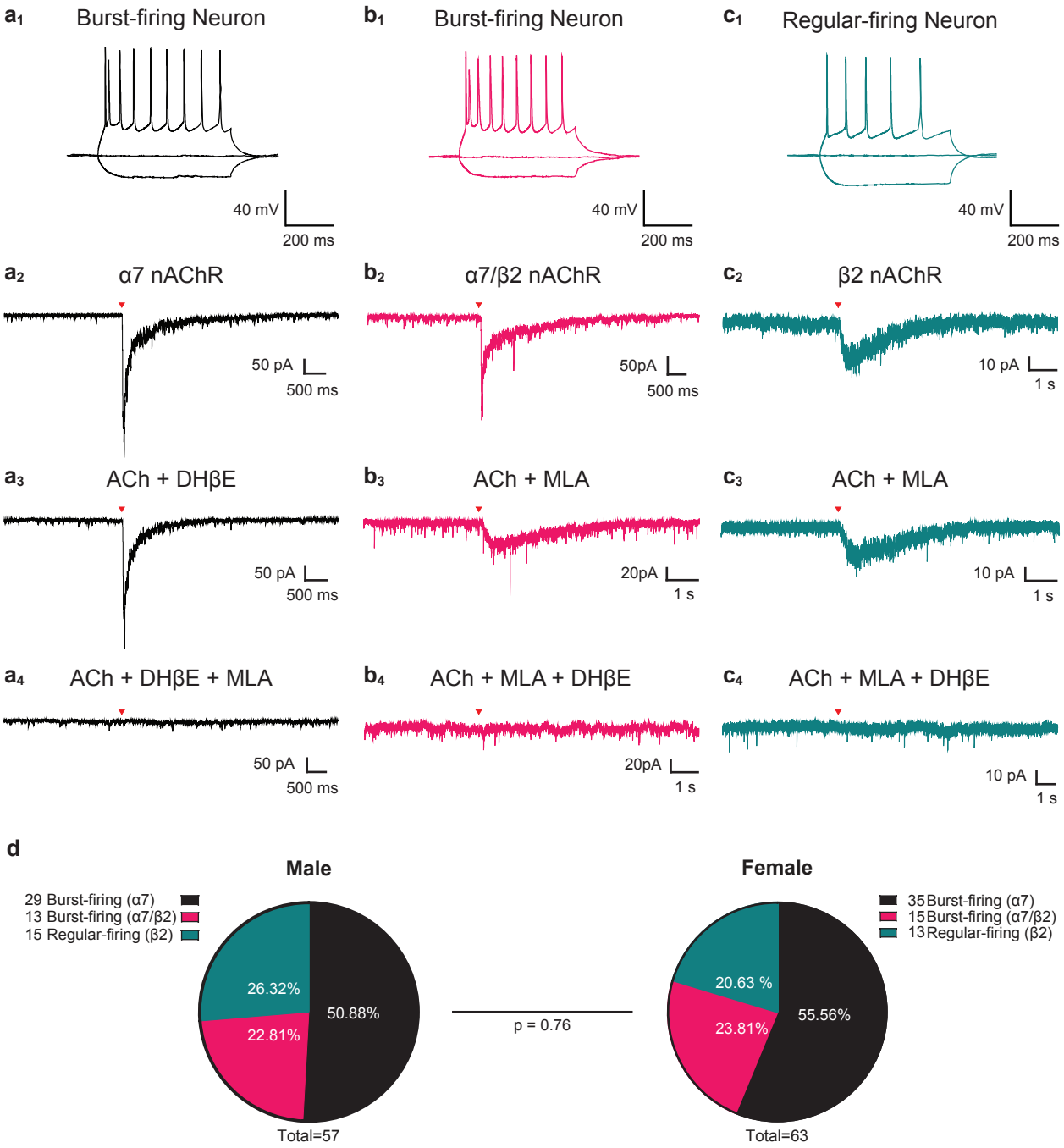
a1
Burst-firing Neuron
40 mV
200 ms
b1
Burst-firing Neuron
40 mV
200 ms
c1
Regular-firing Neuron
40 mV
200 ms
a2
α7 nAChR
50 pA
500 ms
b2
α7/β2 nAChR
50pA
500 ms
c2
β2 nAChR
10 pA
1 s
a3
ACh + DHβE
50 pA
500 ms
b3
ACh + MLA
20pA
1 s
c3
ACh + MLA
10 pA
1 s
a4
ACh + DHβE + MLA
50 pA
500 ms
b4
ACh + MLA + DHβE
20pA
1 s
c4
ACh + MLA + DHβE
10 pA
1 s
d
Male
29 Burst-firing (α7)
13 Burst-firing (α7/β2)
15 Regular-firing (β2)
26.32%
50.88%
22.81%
Total=57
p = 0.76
Female
35 Burst-firing (α7)
15 Burst-firing (α7/β2)
13 Regular-firing (β2)
20.63 %
55.56%
23.81%
Total=63

Figure 2

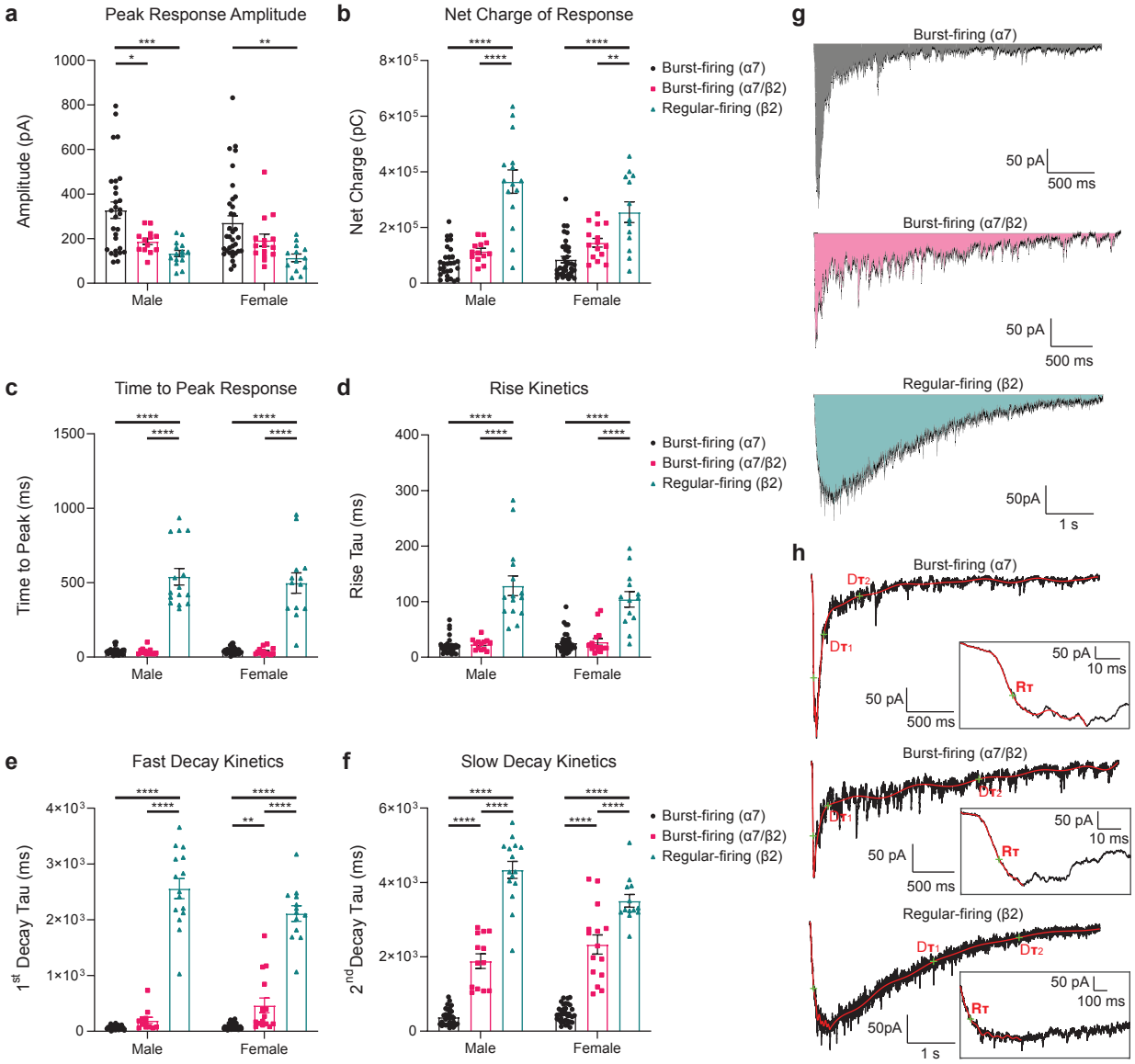
a
Peak Response Amplitude
Amplitude (pA)
Male
Female
b
Net Charge of Response
Net Charge (pC)
Burst-firing (α7)
Burst-firing (α7/β2)
Regular-firing (β2)
c
Time to Peak Response
Time to Peak (ms)
d
Rise Kinetics
Rise Tau (ms)
e
Fast Decay Kinetics
1st Decay Tau (ms)
f
Slow Decay Kinetics
2nd Decay Tau (ms)
g
Burst-firing (α7)
50 pA
500 ms
Burst-firing (α7/β2)
Regular-firing (β2)
50pA
1 s
h
DT2
DT1
RT
10 ms
100 ms

Figure 3

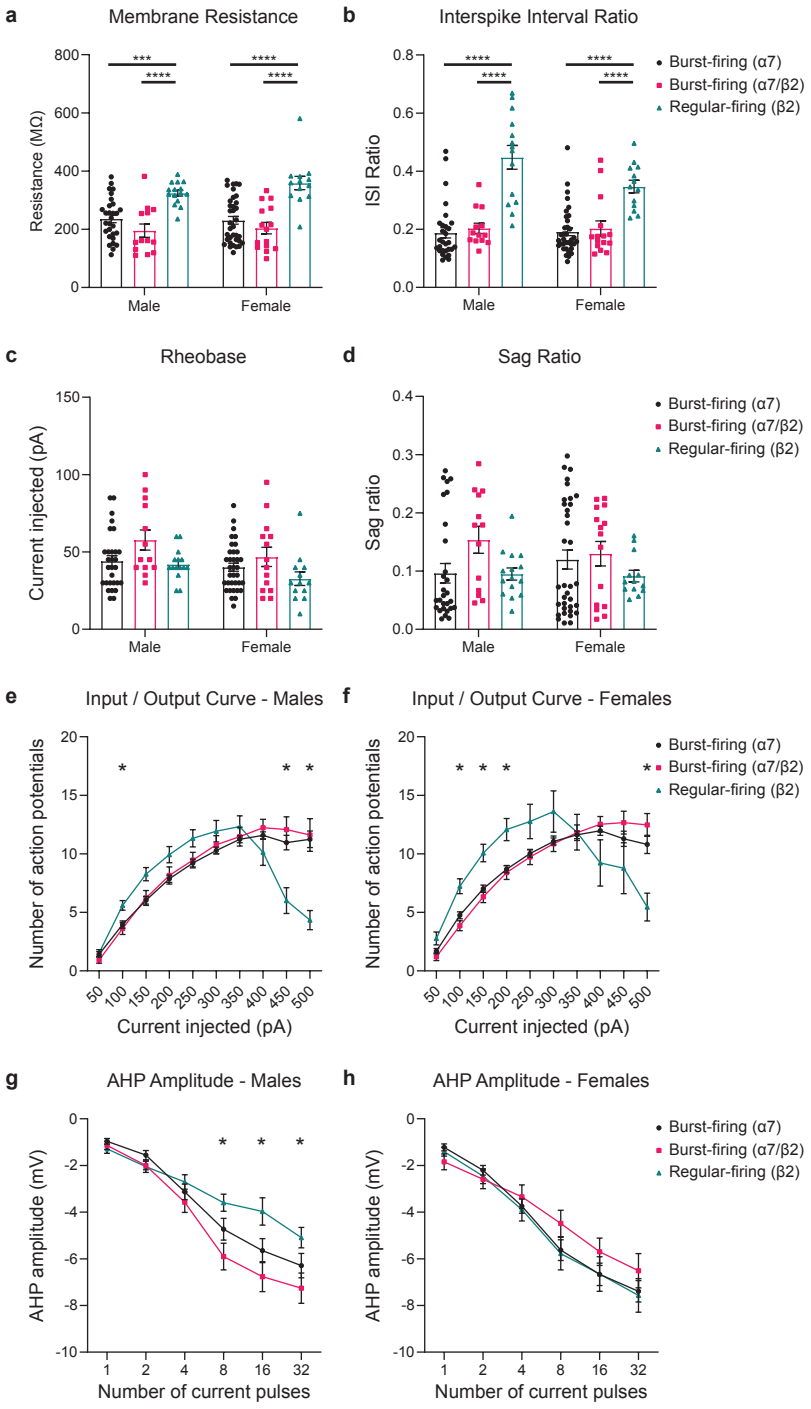
a
Membrane Resistance
Resistance (MΩ)
800
600
400
200
0
***
****
****
****
Male
Female
b
Interspike Interval Ratio
ISI Ratio
0.8
0.6
0.4
0.2
0.0
****
****
****
****
Male
Female
Burst-firing (α7)
Burst-firing (α7/β2)
Regular-firing (β2)
c
Rheobase
Current injected (pA)
150
100
50
0
Male
Female
d
Sag Ratio
Sag ratio
0.4
0.3
0.2
0.1
0.0
Male
Female
Burst-firing (α7)
Burst-firing (α7/β2)
Regular-firing (β2)
e
Input / Output Curve - Males
Number of action potentials
20
15
10
5
0
*
* *
50 100 150 200 250 300 350 400 450 500
Current injected (pA)
f
Input / Output Curve - Females
Number of action potentials
20
15
10
5
0
* * *
*
50 100 150 200 250 300 350 400 450 500
Current injected (pA)
Burst-firing (α7)
Burst-firing (α7/β2)
Regular-firing (β2)
g
AHP Amplitude - Males
AHP amplitude (mV)
0
-2
-4
-6
-8
-10
* * *
1 2 4 8 16 32
Number of current pulses
h
AHP Amplitude - Females
AHP amplitude (mV)
0
-2
-4
-6
-8
-10
1 2 4 8 16 32
Number of current pulses
Burst-firing (α7)
Burst-firing (α7/β2)
Regular-firing (β2)

Figure 4

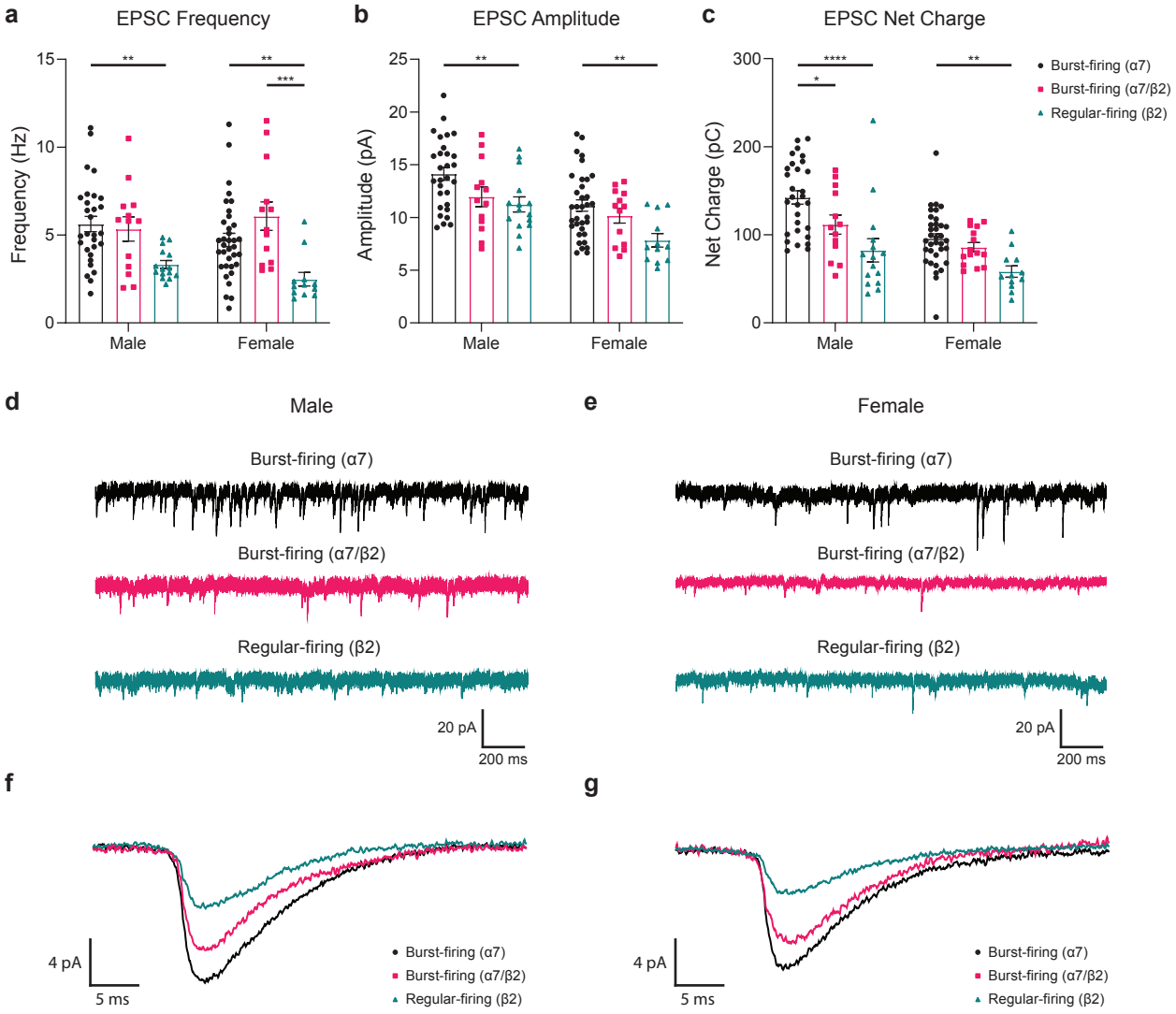
a
EPSC Frequency
Frequency (Hz)
15
10
5
0
**
**
***
Male
Female
b
EPSC Amplitude
Amplitude (pA)
25
20
15
10
5
0
**
**
Male
Female
c
EPSC Net Charge
Net Charge (pC)
300
200
100
0
****
*
**
Male
Female
Burst-firing (α7)
Burst-firing (α7/β2)
Regular-firing (β2)
d
Male
Burst-firing (α7)
Burst-firing (α7/β2)
Regular-firing (β2)
20 pA
200 ms
e
Female
Burst-firing (α7)
Burst-firing (α7/β2)
Regular-firing (β2)
20 pA
200 ms
f
4 pA
5 ms
Burst-firing (α7)
Burst-firing (α7/β2)
Regular-firing (β2)
g
4 pA
5 ms
Burst-firing (α7)
Burst-firing (α7/β2)
Regular-firing (β2)

Figure 5

a

Electrophysiology Correlation Matrix

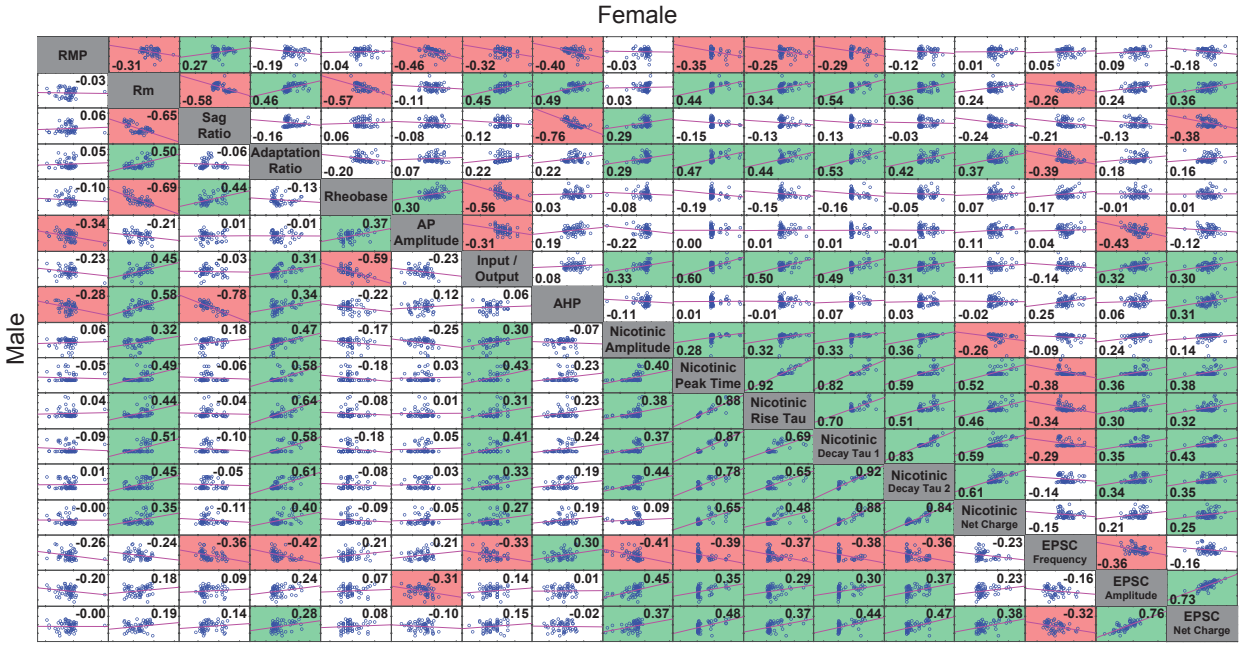

b

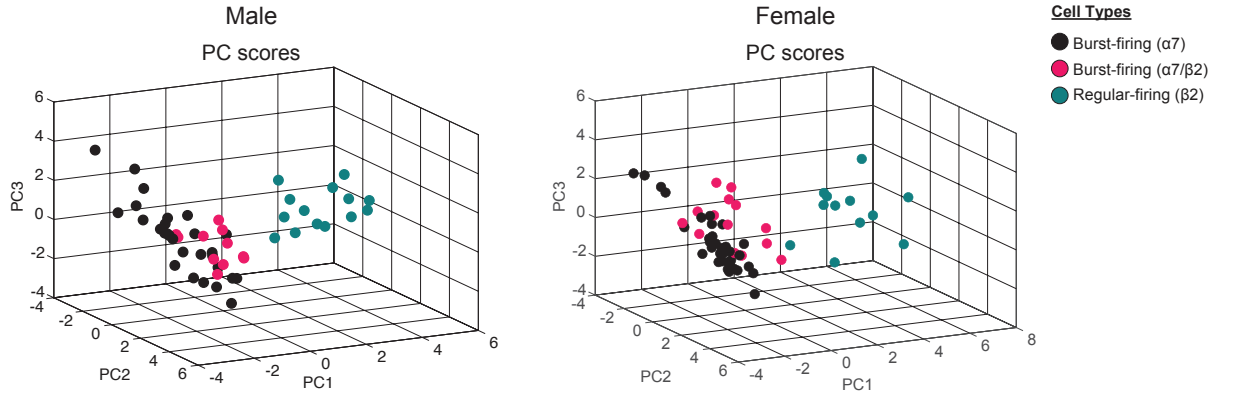

Figure 6

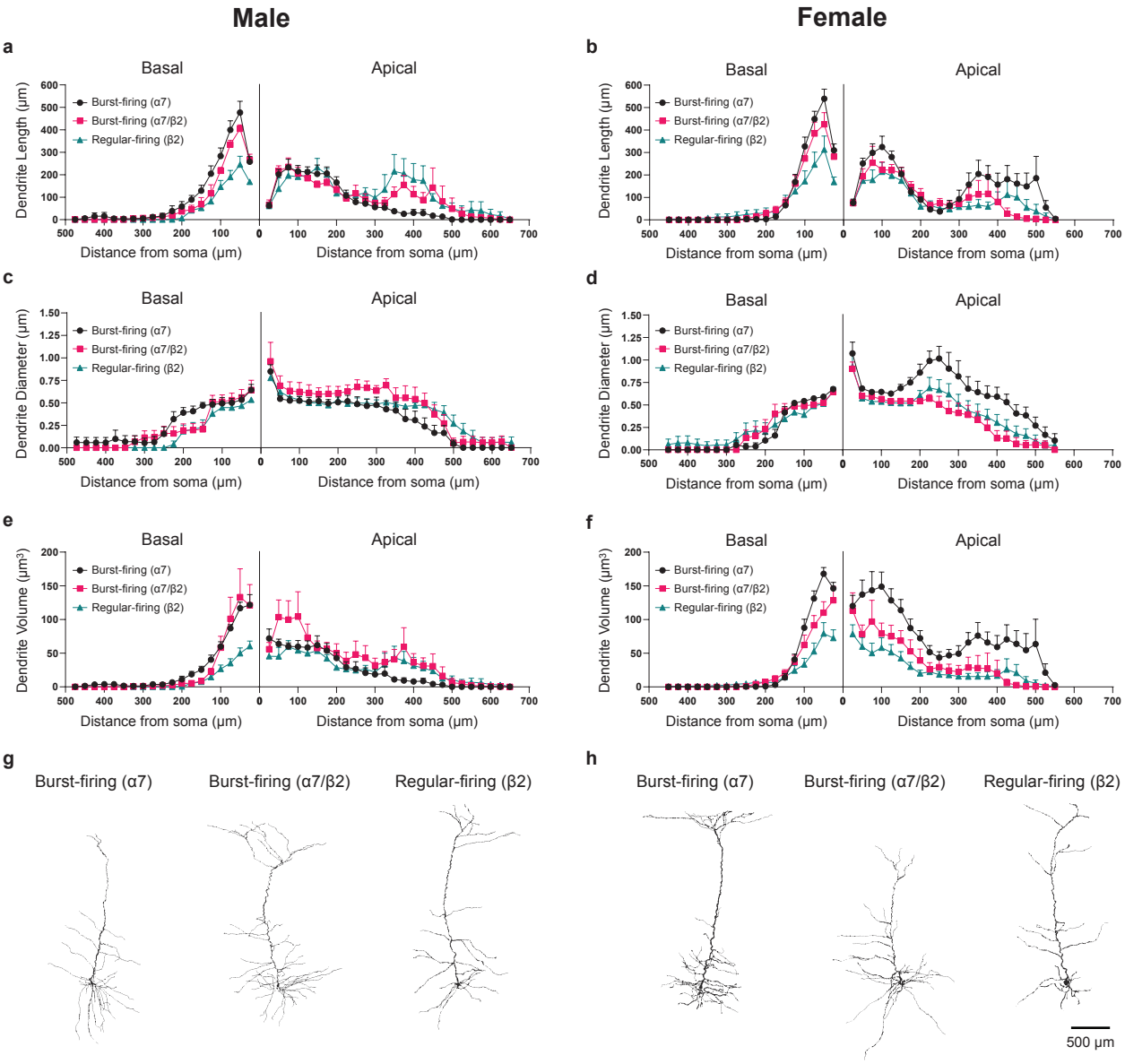
Male
Female
a
b
c
d
e
f
g
h
Basal
Apical
Dendrite Length (µm)
Dendrite Diameter (µm)
Dendrite Volume (µm³)
Burst-firing (α7)
Burst-firing (α7/β2)
Regular-firing (β2)
Distance from soma (µm)
500 µm

Figure 7

a

Burst-firing (α7)

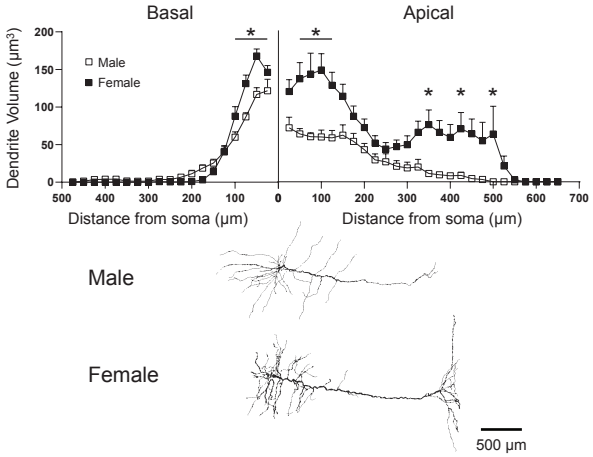

b

Burst-firing (α7/β2)

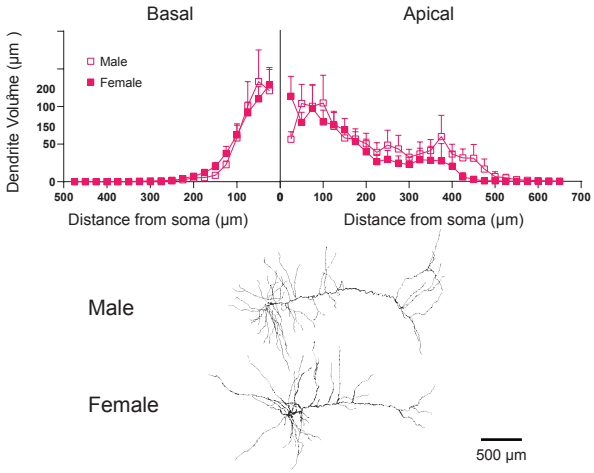

c

Regular-firing (β2)

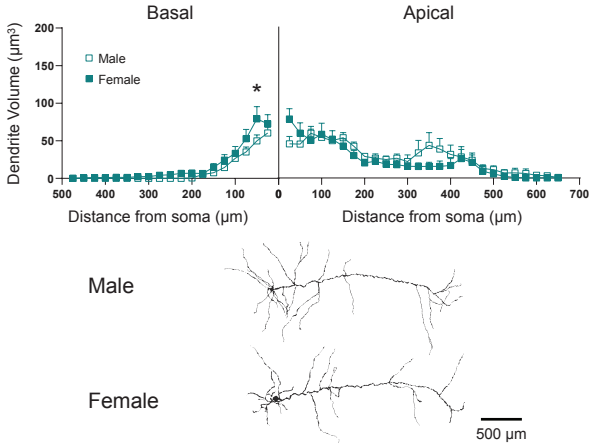

Figure 8

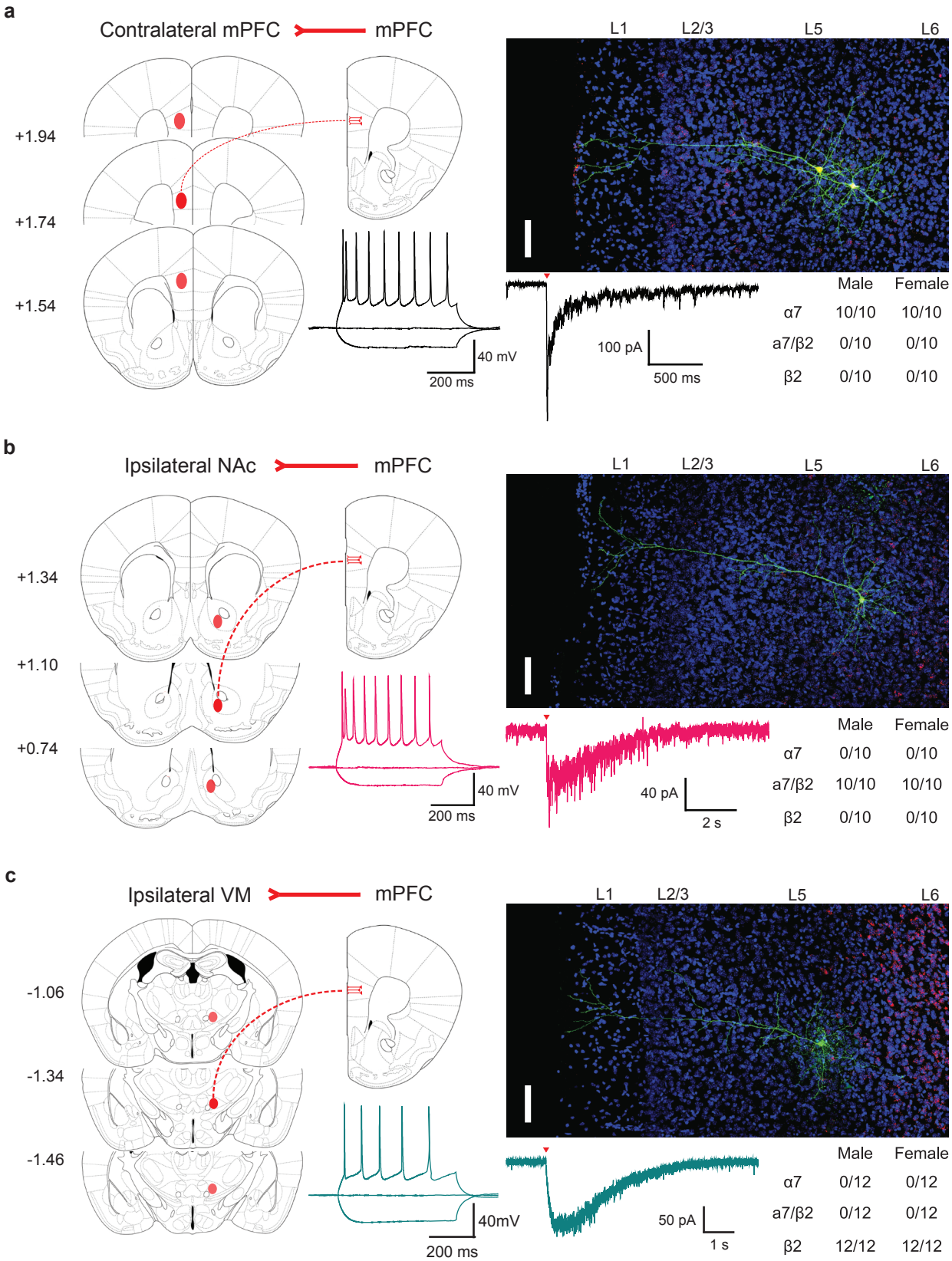
a
Contralateral mPFC
mPFC
+1.94
+1.74
+1.54
40 mV
200 ms
L1
L2/3
L5
L6
100 pA
500 ms
Male Female
α7 10/10 10/10
a7/β2 0/10 0/10
β2 0/10 0/10
b
Ipsilateral NAc
mPFC
+1.34
+1.10
+0.74
40 mV
200 ms
L1
L2/3
L5
L6
40 pA
2 s
Male Female
α7 0/10 0/10
a7/β2 10/10 10/10
β2 0/10 0/10
c
Ipsilateral VM
mPFC
-1.06
-1.34
-1.46
40mV
200 ms
L1
L2/3
L5
L6
50 pA
1 s
Male Female
α7 0/12 0/12
a7/β2 0/12 0/12
β2 12/12 12/12

Figure 9

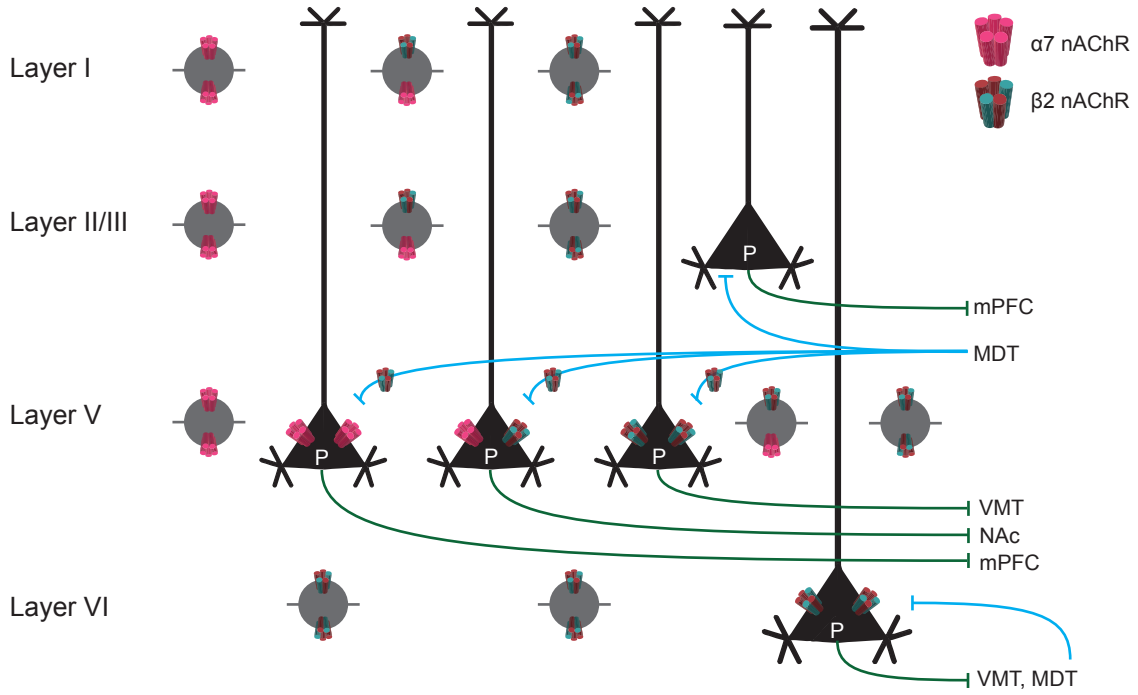
Layer I
Layer II/III
Layer V
Layer VI
α7 nAChR
β2 nAChR
P
mPFC
MDT
VMT
NAc
mPFC
VMT, MDT